iScience

CellPress
OPEN ACCESS

Article

Cancer-associated fibroblasts promote enzalutamide resistance and PD-L1 expression in prostate cancer through CCL5-CCR5 paracrine axis

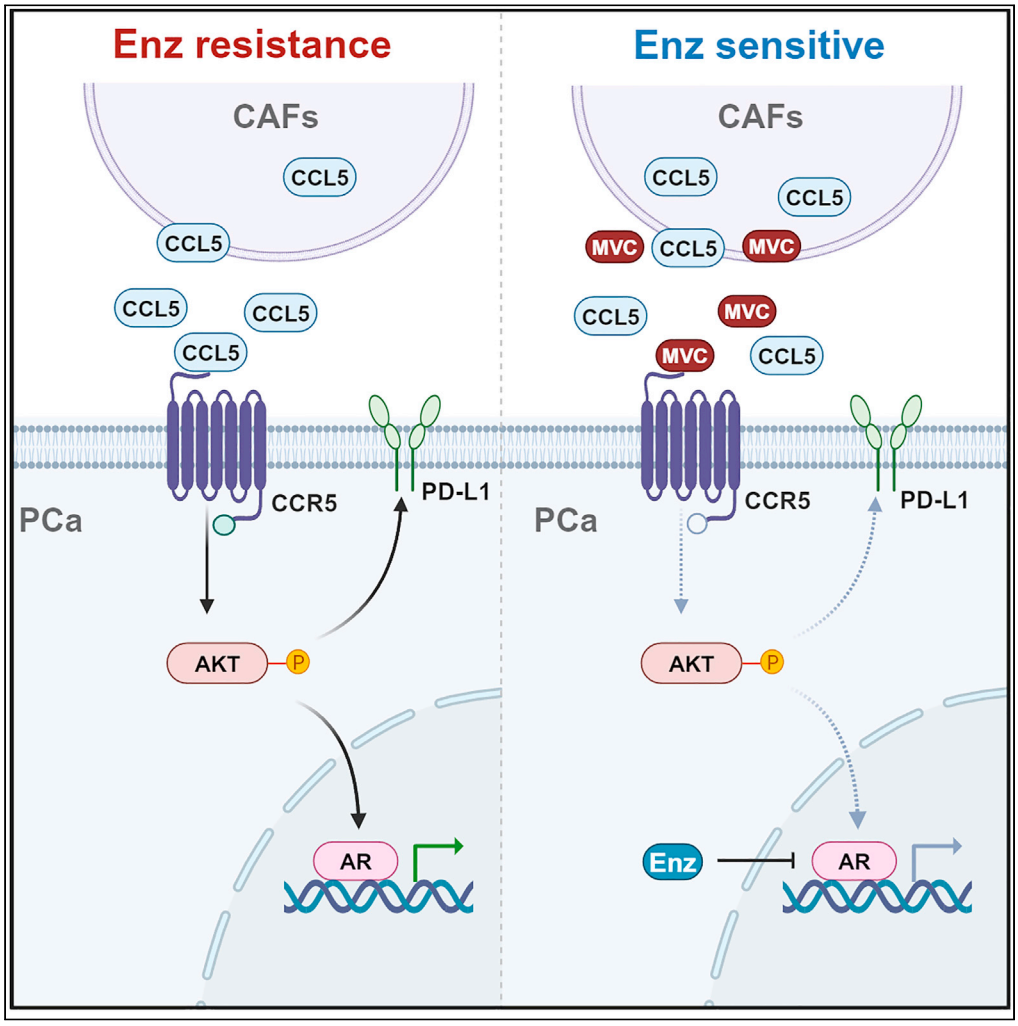

Zhi Xiong, Shun-Li Yu, Zhao-Xiang Xie, ..., Jun-Jia Xie, Hai Huang, Kai-Wen Li

huangh9@mail.sysu.edu.cn (H.H.)
likw6@mail.sysu.edu.cn (K.-W.L.)

Highlights

CAFs upregulate the expression of AR and PD-L1 by activating the AKT signaling pathway

CCL5-CCR5 paracrine axis mediates the interaction between CAFs and PCa cells

Blocking the CCL5-CCR5 axis with the CCR5 antagonist MVC enhances the effect of Enz

Xiong et al., iScience 27, 109674
May 17, 2024
https://doi.org/10.1016/j.isci.2024.109674

iScience

CellPress
OPEN ACCESS

Article

Cancer-associated fibroblasts promote enzalutamide resistance and PD-L1 expression in prostate cancer through CCL5-CCR5 paracrine axis

Zhi Xiong,[1,2,7] Shun-Li Yu,[1,2,7] Zhao-Xiang Xie,[1,2,7] Rui-Lin Zhuang,[1,2] Shi-Rong Peng,[1,2] Qiong Wang,[3] Ze Gao,[4] Bing-Heng Li,[1,2] Jun-Jia Xie,[1,2] Hai Huang,[1,2,5,6,8,*] and Kai-Wen Li[1,2,*]

SUMMARY

Cancer-associated fibroblasts (CAFs) have been shown to play a key role in prostate cancer treatment resistance, but the role of CAFs in the initial course of enzalutamide therapy for prostate cancer remains unclear. Our research revealed that CAFs secrete CCL5, which promotes the upregulation of androgen receptor (AR) expression in prostate cancer cells, leading to resistance to enzalutamide therapy. Furthermore, CCL5 also enhances the expression of tumor programmed death-ligand 1 (PD-L1), resulting in immune escape. Mechanistically, CCL5 binds to the receptor CCR5 on prostate cancer cells and activates the AKT signaling pathway, leading to the upregulation of AR and PD-L1. The CCR5 antagonist maraviroc to inhibit the CAFs mediated CCL5 signaling pathway can effectively reduce the expression of AR and PD-L1, and improve the efficacy of enzalutamide. This study highlights a promising therapeutic approach targeting the CCL5-CCR5 signaling pathway to improve the effectiveness of enzalutamide.

INTRODUCTION

Prostate cancer (PCa) is a common malignancy and the second leading cause of death among men in Western countries.[1] Advanced PCa is primarily treated with androgen deprivation therapy (ADT); however, there is currently no cure for the eventual development of resistance to ADT resistance.[2,3] Second-generation antiandrogens, such as enzalutamide (Enz), have shown significant prolongation of patient survival and promising inhibitory effects.[4,5] However, even with the combination of the most potent inhibitors of androgen receptor (AR) signaling, patients rarely achieve a complete response and eventually develop resistance to Enz.[6] Despite the successful use of immune checkpoint inhibitors (ICIs), particularly the blockade of programmed cell death protein 1/programmed death-ligand 1 (PD-1/PD-L1), in the treatment of other cancers, prostate tumors have proven to be resistant to immunotherapy.[7–9] Therefore, there is an urgent need for an in-depth understanding of the mechanisms of Enz therapy resistance in PCa and the development of new combination therapy strategies for advanced PCa.

The AR is a key factor in the survival of prostate tumors and plays a crucial role in cancer progression and drug resistance.[5] Understanding the mechanisms that enable tumor cell survival is essential for achieving a complete response. Previous studies on resistance to AR-targeted therapy in PCa have primarily focused on intracellular mechanisms.[10–12] However, growing evidence suggests that the tumor microenvironment (TME) also plays an active role in tumor progression.[13–15] In PCa, the presence of tumor-infiltrating B lymphocytes and myeloid-derived suppressor cells (MDSCs) promotes the development of castration-resistant prostate cancer (CRPC) by producing inflammatory cytokines such as IL-23.[16,17] Additionally, fibroblast growth factors (FGFs) contribute to CRPC through autocrine or paracrine signaling.[18] NRG1, originating from the tumor microenvironment, activates the HER3 signaling pathway, leading to the activation of AR downstream target proteins and promoting resistance to antiandrogen therapy in PCa.[19]

Activated stromal cells, commonly referred to as cancer-associated fibroblasts (CAFs), play a significant role in the TME.[20,21] Compared to normal fibroblasts (NFs), CAFs exhibit overexpression of biomarker proteins including α-smooth muscle actin (α-SMA), fibroblast activation protein (FAP), platelet-derived growth factor receptor α or β (PDGFR-α/β), or vimentin.[22] As the predominant cell type in the TME, CAFs actively contribute to cancer progression.[23,24] The interactions between CAFs and tumor cells primarily promote tumorigenesis through the secretion of various proteins (such as TGF-β, IGF, and IL6), direct interaction with tumor cells, modulation of the immune response,

[1]Department of Urology, Sun Yat-sen Memorial Hospital, Sun Yat-sen University, Guangzhou 510120, China
[2]Guangdong Provincial Key Laboratory of Malignant Tumor Epigenetics and Gene Regulation, Sun Yat-Sen Memorial Hospital, Sun Yat-Sen University, Guangzhou 510120, China
[3]Department of Urology, Southern Medical University Nanfang Hospital, Guangzhou 510120, China
[4]Department of Urology, Qilu Hospital of Shandong University, Jinan 250063, China
[5]Guangdong Provincial Clinical Research Center for Urological Diseases, Sun Yat-Sen Memorial Hospital, Sun Yat-Sen University, Guangzhou 510120, China
[6]Department of Urology, The Sixth Affiliated Hospital of Guangzhou Medical University, Qingyuan People's Hospital, Qingyuan 511518, Guangdong, China
[7]These authors contributed equally
[8]Lead contact
*Correspondence: huangh9@mail.sysu.edu.cn (H.H.), likw6@mail.sysu.edu.cn (K.-W.L.)
https://doi.org/10.1016/j.isci.2024.109674

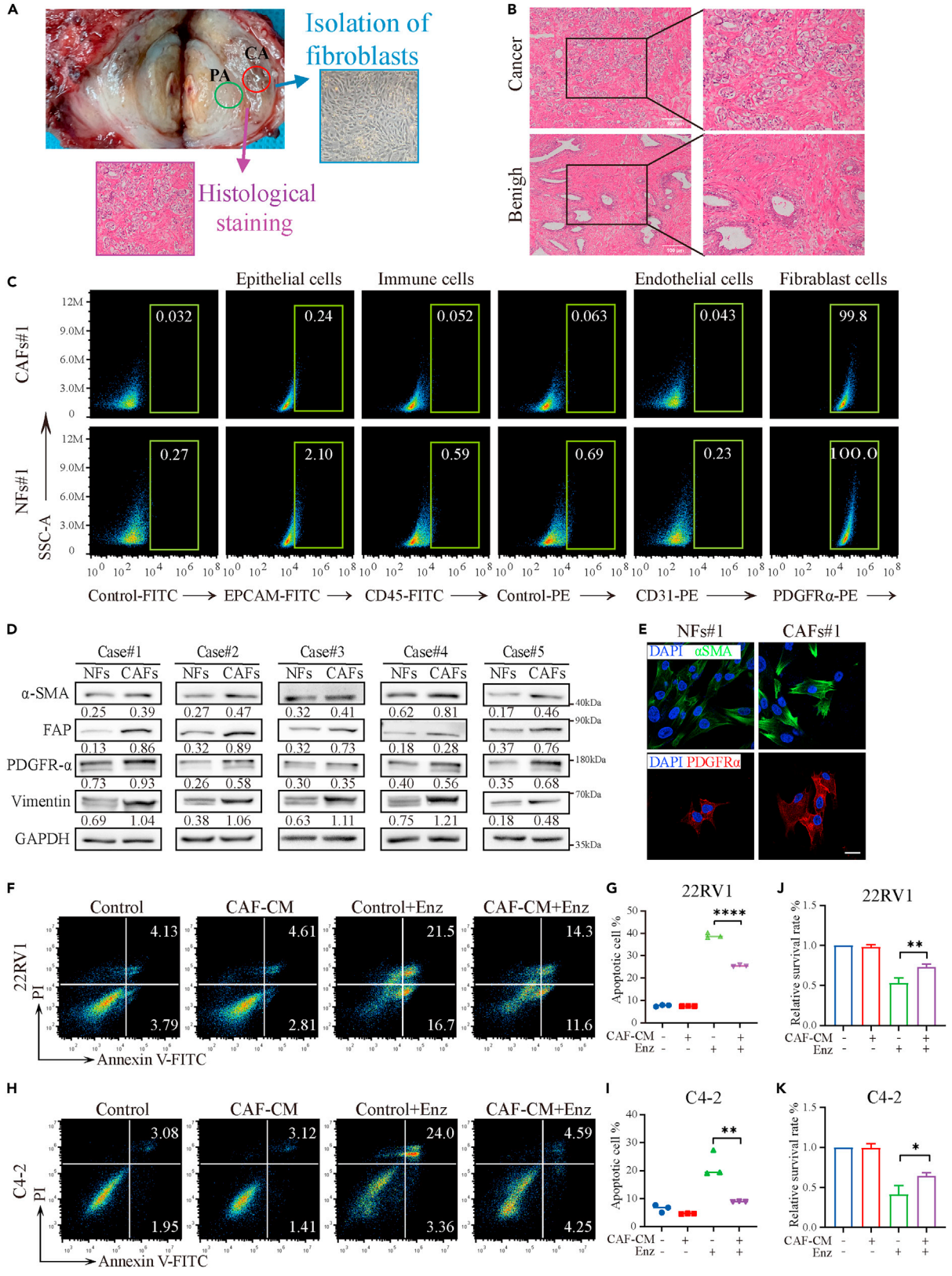
A
CA
PA
Isolation of fibroblasts
Histological staining
B
Cancer
Benigh
C
Epithelial cells
Immune cells
Endothelial cells
Fibrablast cells
CAFs#1
NFs#1
SSC-A
0.032
0.24
0.052
0.063
0.043
99.8
0.27
2.10
0.59
0.69
0.23
100.0
Control-FITC
EPCAM-FITC
CD45-FITC
Control-PE
CD31-PE
PDGFRα-PE
D
Case#1
Case#2
Case#3
Case#4
Case#5
NFs CAFs
α-SMA
FAP
PDGFR-α
Vimentin
GAPDH
40kDa
90kDa
180kDa
70kDa
35kDa
E
NFs#1
CAFs#1
DAPI αSMA
DAPI PDGFRα
F
Control
CAF-CM
Control+Enz
CAF-CM+Enz
22RV1
PI
Annexin V-FITC
4.13
4.61
21.5
14.3
3.79
2.81
16.7
11.6
G
22RV1
Apoptotic cell %
****
CAF-CM
Enz
J
22RV1
Relative survival rate %
**
H
C4-2
3.08
3.12
24.0
4.59
1.95
1.41
3.36
4.25
I
C4-2
**
K
C4-2
*

Figure 1. CAFs isolated from human PCa protect PCa cells from Enz-induced apoptosis

(A) Schematic diagram of CAFs isolation from human PCa. From radical prostatectomy specimens a tumor and a non-malignant benign tissue punch needle biopsy was extracted by an experienced uropathologist from the contralateral sites of the specimens (green/red circles). While a small portion of the extracted tissue cores was fixed and used for histological stains and confirmation of the tissue's identity, the rest was used immediately for CAFs isolated by Enzymatic digestion.

(B) Representative hematoxylin and eosin staining (HE). Scale bar: 100 μm.

(C) Flow cytometry analysis of CAFs isolated from normal adjacent tissue and the tumor-derived from PCa patients showed that the purity of the CAFs was high. CAF preparations displayed a good expression of CAF markers PDGFRα and undetected or low level of endothelial cells (marked by CD31) and epithelial cells (marked by EPCAM) as well as immune cells (marked by CD45).

(D) Representative western blot image of PDGFRα, αSMA, FAP, and vimetin in NFs and CAFs.

(E) Immunofluorescent staining analysis of the fibroblast marker (αSMA and PDGFRα) expression in NFs and CAFs. Scale bar: 20 μm.

(F–I) Apoptosis analysis of PCa cells with indicated treatments. 22RV1 and C4-2 cells were stimulated with CAF-CM or the control medium for 24 h followed by the administration of Enz (10 μM) or DMSO for 24 h. $n = 3$ biologically independent CAFs samples.

(J and K) Cell survival analysis of PCa cells with indicated treatments. 22RV1 and C4-2 cells were stimulated with CAF-CM or the control medium for 24 h followed by the administration of ENZ (10 μM) or DMSO for 24 h. $n = 3$ biologically independent CAFs samples. Data are reported as the mean ± SEM. *$p < 0.05$, **$p < 0.01$, ***$p < 0.001$, ****$p < 0.0001$. One-way ANOVA with Tukey's test for pairwise comparisons for statistical significance analysis in Figures 1G and 1I–1K.

and remodeling of the extracellular matrix (ECM).[23,25] However, further research is required to understand the clinical role, biological function, and mechanism of action of CAFs in prostate cancer; particularly in the context of ADT or immunotherapy. Therefore, additional studies are needed to investigate how CAFs affect the responsiveness of prostate cells to AR-targeted therapies.

In this study, we demonstrate that CAFs-secreted CC motif chemokine ligand 5 (CCL5) activates CC motif chemokine receptor 5 (CCR5) to increase the expression of AR and PD-L1 expression in PCa. This results in resistance to Enz treatment and immune evasion. We also investigate the therapeutic potential of targeting the paracrine axis of CCL5-CCR5 via maraviroc (MVC), an FDA-approved CCR5 antagonist that is widely employed in the treatment of acquired immunodeficiency syndrome (AIDS). The results of our study demonstrate that targeting the CCL5-CCR5 axis can significantly augment the effectiveness of Enz in combating PCa.

RESULTS

CAFs protect PCa cells from Enz-induced cytotoxicity

CAFs in the TME are considered to play a beneficial role in promoting tumor survival.[21,23,25] We collected specimens from 30 patients with PCa who underwent radical prostatectomy and isolated samples of both benign and malignant prostate samples. To minimize any potential on-site effects (Figure 1A), the benign samples were kept separate from the tumors. Detailed information on the patients and their tumors is provided in Table S1. Each biopsy specimen was histopathologically examined, and primary fibroblasts were isolated by enzymatic digestion (Figures 1A and 1B). A total of 16 pairs of fibroblasts were successfully isolated. To confirm the purity of the patient-matched tumor-adjacent NFs and CAFs, we conducted flow cytometry experiments on the isolated NFs and CAFs. The fibroblast marker PDGFRα was expressed by NFs and CAFs, while the endothelial marker CD31, immune cell marker CD45, and epithelial cell marker EPCAM were not detected (Figure 1C). To further distinguish NFs from CAFs, we performed western blot and immunofluorescence experiments, which revealed significantly higher expression levels of the markers αSMA, FAP, vimentin, and PDGFRα in CAFs compared to NFs (Figures 1D, 1E, and S1).

Studies have indicated that CAFs may play a crucial role in influencing resistance to endocrine therapy in PCa.[19] CAFs primarily exert their effects through two pathways: direct interaction with tumor cells and the regulation of biological functions through paracrine signaling. To assess whether CAFs modulate the response of PCa cells to Enz through paracrine stimulation, we obtained the conditioned medium from primary CAFs (CAF-CM) and added it to AR-positive androgen-independent PCa cell lines (22RV1 and C4-2 cells). The results demonstrated a significant decrease in the proportion of apoptotic Enz-treated 22RV1 and C4-2 cells after CAF-CM treatment (Figures 1F–1I). Consistently, the survival rate of Enz-treated 22RV1 and C4-2 cells showed a notable increase following CAF-CM stimulation (Figures 1J and 1K). Collectively, these findings suggest that CAFs cf. protection to PCa cells against Enz-induced cytotoxicity in a cell-nonautonomous manner.

CCL5 is upregulated in CAFs compared to NFs

To investigate the protective mechanism of CAFs against Enz-induced cytotoxicity in PCa cells, we conducted a transcriptome analysis comparing matched NFs and CAFs in three groups of patients. We identified 168 genes that showed significantly differential expression between NFs and CAFs ($p < 0.05$, log-fold change; Figure S2A). Subsequently, we performed gene set enrichment analysis (GSEA) to determine the molecular pathways and biological processes involved. Our findings revealed the upregulation of pathways such as cytokine-cytokine receptor interactions in CAFs (Figure 2A). Notably, we observed upregulation of CCL5, a chemokine associated with immune regulation, in CAFs compared to NFs (Figure S2A). Moreover, in the TCGA-PRAD dataset, we established a clear correlation between CCL5 and CAF markers (PDGFRA, ACTA2, VIM, and FAP) (Figure 2B). Furthermore, the expression of CCL5 was higher in tumor tissues than in normal prostate tissues in the TCGA-PRAD dataset (Figure S2B).

To assess the clinical relevance of CCL5, we conducted RT-qPCR on 30 PCa and paracancerous tissue samples to determine the expression patterns of CCL5. The findings revealed that CCL5 expression was higher in tumors than in the matched paracancerous tissues (Figure 2C). Additionally, RT-qPCR and immunofluorescence experiments confirmed that CCL5 expression in CAFs was significantly higher in CAFs than in NFs (Figures 2D and 2E). By comparing the levels of CCL5 in conditioned medium from NFs (NF-CM) and CAF-CM using ELISA, we confirmed

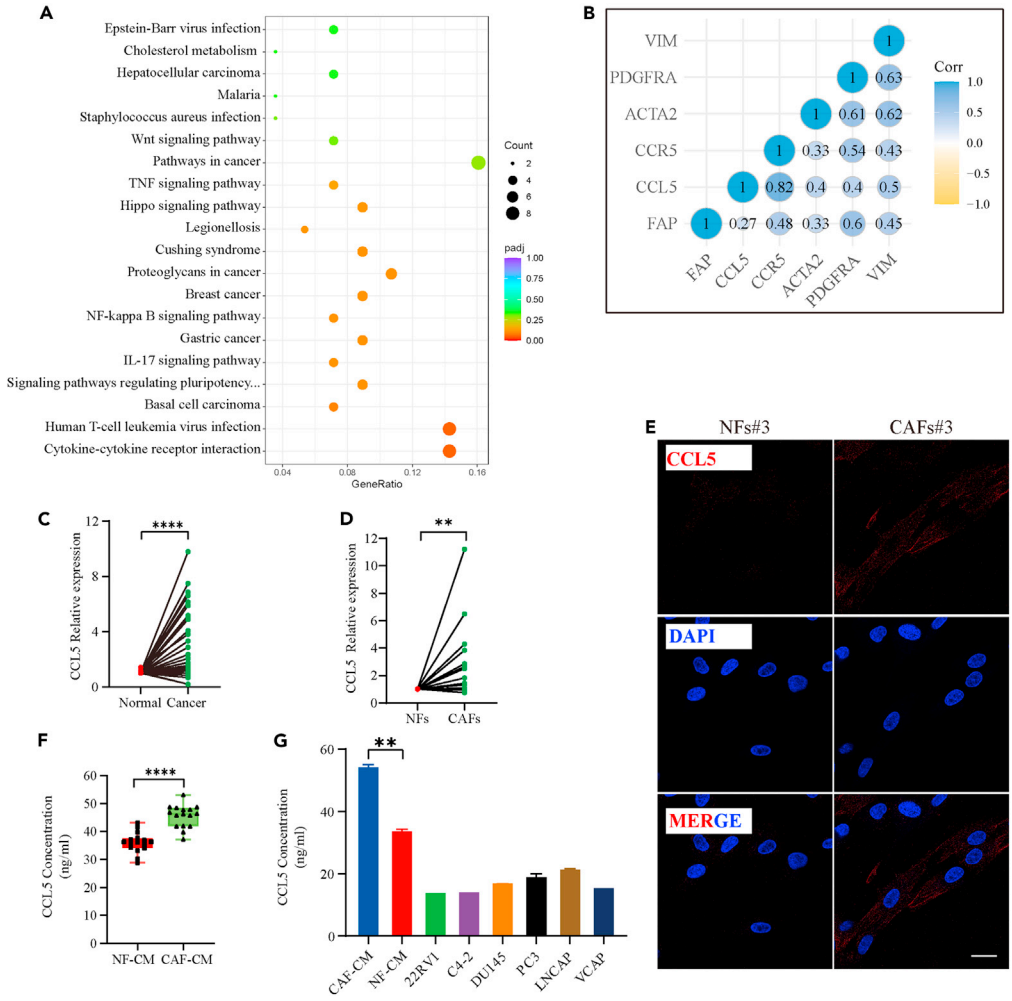

Figure 2. High CCL5 expression in CAFs

(A) Pathways that were significantly enriched between these two cell types. Each node (circle) represents a pathway while the edges (lines) connecting nodes show the shared genes between pathways with the thickness of the edge corresponding to degree of sharing. Color of node indicates positive (red) or negative (green) enrichment in CAFs.

(B) Bivariate correlation analysis showing positive correlations of CCL5 or CCR5 and CAFs markers FAP, PDGFRA, VIM, and ACTA2 expression in PCa from the TCGA database.

(C) The expression of CCL5 between normal adjacent tissue and PCa tissues in our cohort (n = 30) by RT-qPCR analyses.

(D) The expression of CCL5 between paired NFs and CAFs (n = 16 pairs) by RT-qPCR analyses.

(E) Immunofluorescent staining analysis of the CCL5 expression in NFs and CAFs. Scale bar: 20 μm.

(F) ELISA of CCL5 level in NFs and CAFs (n = 16 pairs).

(G) ELISA of CCL5 level in CAFs, NFs, and PCa cells (22RV1, C4-2, PC3, DU145, LNCAP, VCAP) (n = 2). Data are reported as the mean ± SEM. *$p < 0.05$, **$p < 0.01$, ***$p < 0.001$, ****$p < 0.0001$. Two-tailed unpaired t test for statistical significance analysis in Figures 2C–2F. One-way ANOVA with Tukey's test for pairwise comparisons for statistical significance analysis in Figure 2G.

a significant increase to higher level of CCL5 secretion in CAFs (Figure 2F). Further, ELISA experiments demonstrated that CCL5 was primarily produced by CAFs in PCa, rather than by tumor cells, as evidenced by measurements in the conditioned medium of CAFs, NFs, and various PCa cell lines (22RV1, C4-2, PC3, DU145, LNCAP, and VCAP cells) (Figure 2G). Overall, CCL5 expression was significantly upregulated in CAFs compared with PCa and NFs.

CCL5 enhances resistance of PCa cells to Enz

To investigate the role of CCL5 in PCa cells, we conducted an annexinV FITC/PI double-staining assay to assess apoptosis in 22RV1 and C4-2 cells. The findings revealed that compared to Enz treatment alone, stimulation with recombinant human CCL5 substantially reduced the apoptosis rate of tumor cells (Figures 3A–3D). Furthermore, we selected 22RV1 and C4-2 cells and evaluated their viability using CCK-8

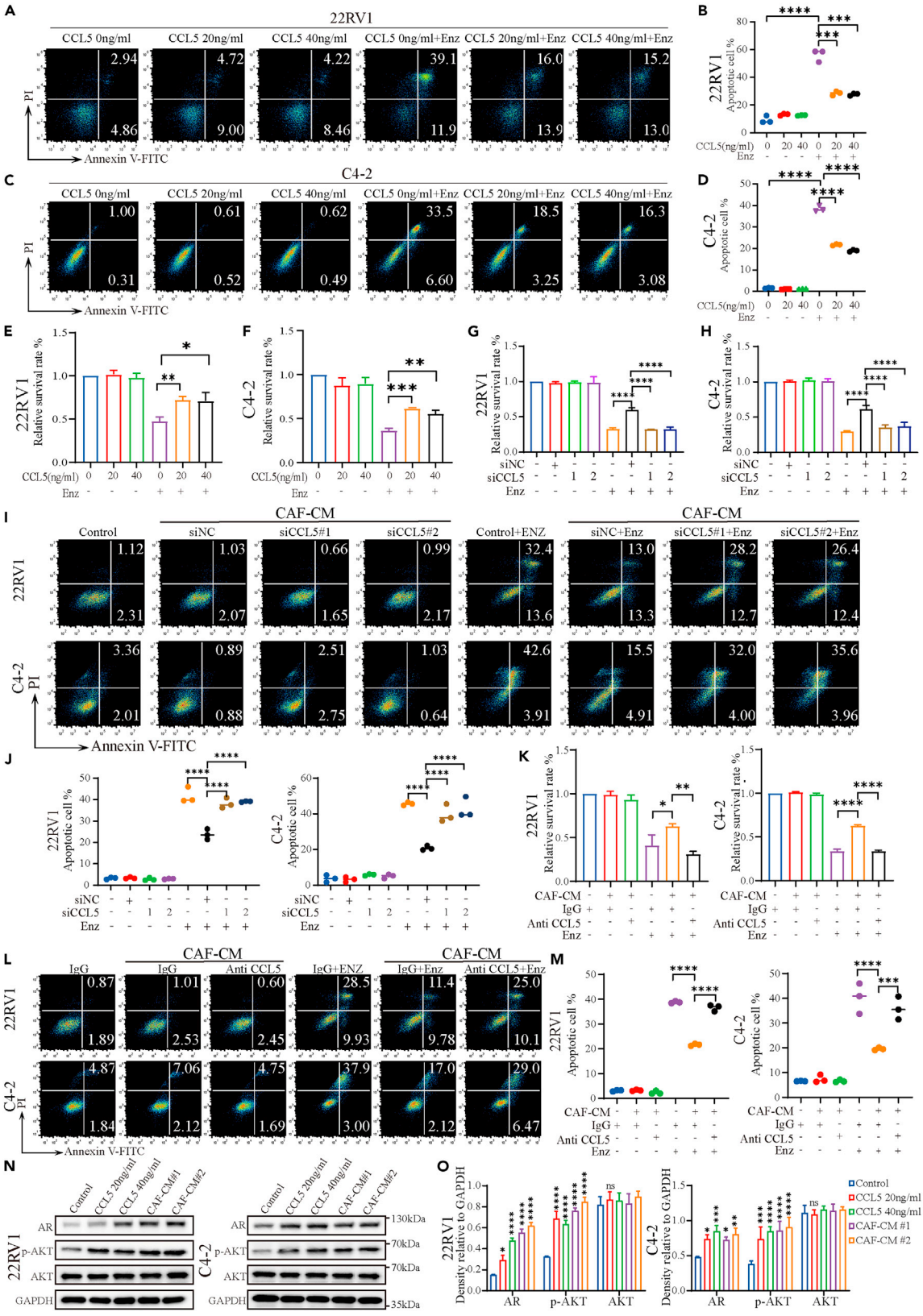
A
22RV1
CCL5 0ng/ml
CCL5 20ng/ml
CCL5 40ng/ml
CCL5 0ng/ml+Enz
CCL5 20ng/ml+Enz
CCL5 40ng/ml+Enz
2.94
4.72
4.22
39.1
16.0
15.2
4.86
9.00
8.46
11.9
13.9
13.0
PI
Annexin V-FITC
B
22RV1
Apoptotic cell %
CCL5(ng/ml) 0 20 40 0 20 40
Enz - - - + + +
C
C4-2
1.00
0.61
0.62
33.5
18.5
16.3
0.31
0.52
0.49
6.60
3.25
3.08
D
C4-2
E
22RV1
Relative survival rate %
F
C4-2
G
22RV1
siNC - + - - - + - -
siCCL5 - - 1 2 - - 1 2
Enz - - - + + + + +
H
C4-2
I
Control
siNC
siCCL5#1
siCCL5#2
Control+ENZ
siNC+Enz
siCCL5#1+Enz
siCCL5#2+Enz
CAF-CM
1.12
1.03
0.66
0.99
32.4
13.0
28.2
26.4
2.31
2.07
1.65
2.17
13.6
13.3
12.7
12.4
3.36
0.89
2.51
1.03
42.6
15.5
32.0
35.6
2.01
0.88
2.75
0.64
3.91
4.91
4.00
3.96
Annexin V-FITC
J
22RV1
Apoptotic cell %
C4-2
K
22RV1
Relative survival rate %
CAF-CM - + + - + +
IgG + + - + + -
Anti CCL5 - - + - - +
Enz - - - + + +
C4-2
L
IgG
IgG
Anti CCL5
IgG+ENZ
IgG+Enz
Anti CCL5+Enz
0.87
1.01
0.60
28.5
11.4
25.0
1.89
2.53
2.45
9.93
9.78
10.1
4.87
7.06
4.75
37.9
17.0
29.0
1.84
2.12
1.69
3.00
2.12
6.47
M
22RV1
Apoptotic cell %
C4-2
N
Control
CCL5 20ng/ml
CCL5 40ng/ml
CAF-CM#1
CAF-CM#2
22RV1
C4-2
AR
p-AKT
AKT
GAPDH
130kDa
70kDa
70kDa
35kDa
O
22RV1
Density relative to GAPDH
AR
p-AKT
AKT
C4-2
Control
CCL5 20ng/ml
CCL5 40ng/ml
CAF-CM #1
CAF-CM #2

Figure 3. CCL5 activates AR signaling in PCa cells in order to potentiate Enz resistance

(A–D) Apoptosis analysis of 22RV1 and C4-2 cells with indicated treatments. 22RV1 and C4-2 cells were stimulated with CCL5 (20 ng/mL or 40 ng/ml) or vehicle (PBS) for 24 h followed by the administration of Enz (10 μM) or DMSO for 24 h (n = 3).

(E and F) Cell survival analysis of 22RV1 and C4-2 cells with indicated treatments. 22RV1 and C4-2 cells were stimulated with CCL5 (20 ng/mL or 40 ng/ml) or the Control (PBS) for 24 h followed by the administration of Enz (10 μM) or DMSO for 24 h (n = 3).

(G and H) Cell survival analysis of 22RV1 and C4-2 cells with indicated treatments. CM from CAFs expressing siNC or siCCL5 (si-1 or si-2) was collected and added to 22RV1 and C4-2 cells for 24 h. 22RV1 and C4-2 cells were treated with Enz (10 μM) after CM addition for 24 h (n = 3).

(I and J) Apoptosis analysis of 22RV1 and C4-2 cells with indicated treatments. CM from CAFs expressing siNC or siCCL5 (si-1 or si-2) was collected and added to 22RV1 and C4-2 cells for 24 h, and 22RV1 and C4-2 cells were treated with Enz (10 μM) for 24 h. n = 3 biologically independent CAFs samples.

(K) Cell survival analysis of 22RV1 and C4-2 cells with indicated treatments. CAF-CM was pretreated with the neutralizing anti-CCL5 antibody or IgG for 1 h and then added to 22RV1 and C4-2 cells. 22RV1 and C4-2 cells were treated with Enz (10 μM) for 24 h. n = 3 biologically independent CAFs samples.

(L and M) Apoptosis analysis of 22RV1 and C4-2 cells with indicated treatments. CAF-CM was pretreated with the neutralizing anti-CCL5 antibody or IgG for 1 h and then added to 22RV1 and C4-2 cells for 24 h. 22RV1 and C4-2 cells were treated with Enz (10 μM) for 24 h. n = 3 biologically independent CAFs samples.

(N and O) Representative western blot image and quantification of AR, AKT, phosphorylated AKT(Ser473) and GAPDH in 22RV1 and C4-2 cells with indicated treatments for 24 h. Data are reported as the mean ± SEM. ns: no significance, *p < 0.05, **p < 0.01, ***p < 0.001, ****p < 0.0001. One-way ANOVA with Tukey's test for pairwise comparisons for statistical significance analysis in Figure 3B, 3D–3H, 3J, 3K, 3M, and 3O.

reagent after 24 h of stimulation with or without recombinant human CCL5. The results demonstrated that 22RV1 and C4-2 cells treated with CCL5 exhibited greater resistance to Enz than untreated cells (Figures 3E and 3F). These results suggested that CCL5 emulated the protective effects observed with CAF-CM.

Disruption of CCL5 expression in CAFs using siRNA (siCCL5-1 or siCCL5-2) (Figures S2C and S2D) significantly weakened the protective effect of CAF-CM compared to that of the control CM obtained from CAFs expressing non-targeting siRNA (siNC). After knockdown of CCL5 expression in CAFs, the survival rate of Enz-treated PCa cells was significantly reduced (Figures 3G and 3H), and the apoptosis rate was significantly increased (Figures 3I and 3J). Additionally, blocking with a CCL5 neutralizing antibody also partially attenuated the protective effect of CAFs on Enz-treated 22RV1 and C4-2 cells (Figures 3K–3M). These results indicate that CAFs inhibit the sensitivity of PCa cells to Enz predominantly by mediating the CCL5 signaling pathway.

To investigate the underlying mechanism by which CCL5 protects PCa cells from Enz-induced cytotoxicity, we examined the expression levels of AR in PCa cells treated with CM from CAFs or recombinant CCL5. Since reactivation of AR is a common mechanism to Enz therapy,[4,18] we observed a significant increase in AR expression in 22RV1 and C4-2 cells treated with CAF-CM and CCL5 compared to that in control cells (Figures 3N and 3O).

These findings suggested that CAFs shield PCa cells from Enz-induced cytotoxicity by secreting CCL5 in a paracrine manner.

CCL5 and CCR5 together form a paracrine signaling axis to enhance Enz resistance of PCa cells

To determine the interaction between CCL5 and PCa cells, we measured the expression of the important CCL5 receptor, CCR5, in human PCa. To explore the clinical relevance of CCL5 and CCR5, we analyzed their expression in TCGA-PRAD dataset. The results showed that the expression of CCL5 and CCR5 was higher in human PCa tissues than in normal prostate tissues (Figures S2B and S2E). Furthermore, in the TCGA-PRAD dataset, we also observed significant correlations between CCR5 and CCL5 and CAFs markers (PDGFRA, ACTA2, VIM, and FAP) (Figure 2B). Therefore, we speculated that CCL5 from CAFs may interact with PCa cells through the CCR5 receptor, thus constituting a paracrine axis that protects PCa cells from Enz-induced cytotoxicity.

We then verified whether CAFs function by stimulating CCR5 expression in PCa cells. We used siRNAs (siCCR5-1 or siCCR5-2) to disrupt the expression of CCR5 in 22RV1 and C4-2 cells (Figures S3A and S3B). Next, we treated the cells with CAF-CM and subjected them to Enz treatment. Our analysis of apoptosis and cell survival showed that disruption of CCR5 significantly hindered the protective effect of CAFs on PCa cells after Enz treatment (Figures 4A–4F).

To investigate whether blocking the CCL5-CCR5 axis would inhibit the supportive effects of CAFs, we used the CCR5 antagonist MVC. MVC binds to CCR5 and induces conformational changes, preventing ligands from activating CCR5 signaling.[26] We observed that MVC inhibited the protective effect of CAFs on Enz-induced apoptosis and survival in 22RV1 and C4-2 cells (Figures 4G–4L). MVC treatment also inhibited the protective effect of CCL5 against Enz-induced apoptosis (Figures 4M–4P) and PCa cell survival following Enz treatment (Figures 4Q and 4R). In conclusion, MVC disrupts the CCL5-CCR5 axis, significantly weakening the protective effect of CAFs on Enz-induced PCa cells. These findings suggest that the CCL5-CCR5 axis plays a crucial role in mediating the resistance of PCa cells to Enz treatment by CAFs.

The CCL5-CCR5 axis enhances Enz resistance of PCa cells by upregulating AR expression through the AKT signaling pathway

We next investigated the downstream effects of CCL5-CCR5 signaling in PCa cells. Previous studies have shown that in anti-androgen therapy-resistant PCa, there is often an overactivation of the AKT pathway[27] which is associated with CCL5 signaling.[28] We analyzed the TCGA-PRAD dataset and found a significant positive correlation between the CCL5, CCR5, and AKT signaling pathways in human PCa (Figures 5A and 5B). Our experiments demonstrated that stimulation with CAF-CM and CCL5 led to AKT activation in 22RV1 and C4-2 cells, as evidenced by the AKT phosphorylation at serine 473 (Figures 3N and 3O). However, the addition of the CCR5 inhibitor MVC effectively blocked

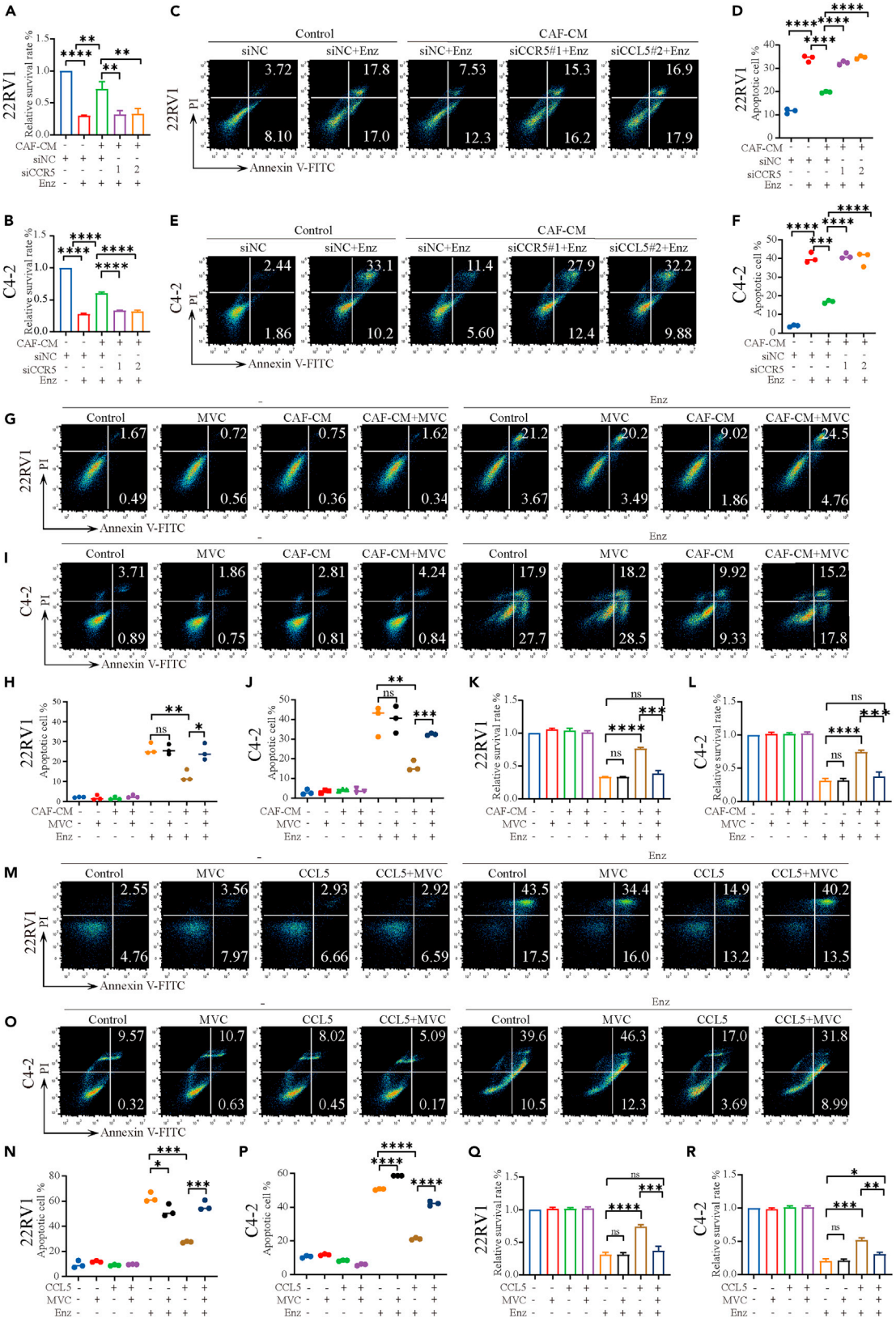
A
22RV1
Relative survival rate %
CAF-CM
siNC
siCCR5
Enz
B
C4-2
C
Control
CAF-CM
siNC
siNC+Enz
siCCR5#1+Enz
siCCL5#2+Enz
PI
Annexin V-FITC
D
Apoptotic cell %
E
F
G
MVC
CAF-CM+MVC
I
H
J
K
L
M
CCL5
CCL5+MVC
O
N
P
Q
R

Figure 4. CAFs enhances the Enz resistance of PCa cells through the CCL5-CCR5 paracrine signaling

(A and B) Cell survival analysis of 22RV1 and C4-2 cells with indicated treatments. 22RV1 and C4-2 cells expressing siNC or siCCR5 (si-1 or si-2) were pretreated with CAF-CM or the control medium for 24 h followed by Enz (10 μM) treatment for 24 h. $n = 3$ biologically independent CAFs samples.

(C–F) Apoptosis analysis of 22RV1 and C4-2 cells with indicated treatments. 22RV1 and C4-2 cells expressing siNC or siCCR5 (si-1 or si-2) were pretreated with CAF-CM or the control medium for 24 h followed by Enz (10 μM) treatment for 24 h. $n = 3$ biologically independent CAFs samples.

(G–J) Apoptosis analysis of 22RV1 and C4-2 cells with indicated treatments. 22RV1 and C4-2 cells were pretreated with MVC (1 μM) or DMSO for 1 h, followed by CAF-CM stimulation for 24 h. Apoptosis analyses were performed 24 h after Enz (10 μM) treatment. $n = 3$ biologically independent CAFs samples.

(K and L) Cell survival analysis of 22RV1 and C4-2 cells with indicated treatments. 22RV1 and C4-2 cells were pretreated with MVC (1 μM) or DMSO for 1 h, followed by CAF-CM stimulation for 24 h. Apoptosis analyses were performed 24 h after Enz (10 μM) treatment. $n = 3$ biologically independent CAFs samples.

(M–P) Apoptosis analysis of 22RV1 and C4-2 cells with indicated treatments. 22RV1 and C4-2 cells were pretreated with MVC (1 μM) or DMSO for 1h, followed by CCL5 (20 ng/mL) stimulation for 24 h. Apoptosis analyses were performed 24 h after Enz (10 μM) treatment ($n = 3$).

(Q and R) Cell survival analysis of 22RV1 and C4-2 cells with indicated treatments. 22RV1 and C4-2 cells were pretreated with MVC (1 μM) or DMSO for 1 h, followed by CCL5 (20 ng/mL) stimulation for 24 h. Apoptosis analyses were performed 24 h after Enz (10 μM) treatment ($n = 3$). Data are reported as the mean ± SEM. ns: no significance, $*p < 0.05$, $**p < 0.01$, $***p < 0.001$, $****p < 0.0001$. One-way ANOVA with Tukey's test for pairwise comparisons for statistical significance analysis in Figures 4A, 4B, 4D–4F, 4H–4L, and 4N–4R.

CAF-mediated AKT activation and AR upregulation (Figures 5C and 5D). Similarly, the CCR5 antagonist MVC significantly inhibited AKT activation and AR upregulation induced by recombinant CCL5 (Figures 5E and 5F). To investigate the role of the AKT pathway in mediating AR expression induced by the CCL5-CCR5 signaling axis, we conducted western blot analysis. The findings revealed that the AKT inhibitor MK-2206 effectively suppressed CCL5-induced AR expression (Figures 5G and 5H).

Collectively, these results indicate that the CCL5-CCR5 signaling pathway can enhance AR expression by activating the AKT signaling pathway, consequently reducing the cytotoxic impact of Enz on PCa cells.

Combination therapy of CCR5 antagonist MVC and Enz inhibits PCa growth

To investigate whether MVC administration could enhance therapeutic efficacy of Enz *in vivo*, we created a subcutaneous xenograft tumor model in which the PCa cell line 22RV1 and CAFs were co-inoculated subcutaneously into immunocompromized nude mice at a ratio of 1:1. Ten days after tumor cell implantation, when the tumor size reached 100 mm^3, the mice were intraperitoneally injected with Enz (10 mg/kg) with or without MVC (10 mg/kg), MVC alone (10 mg/kg), or control solution every three days, and tumor growth was monitored (Figure 6A). Our findings revealed that the animals injected with CAFs and 22RV1 cells exhibited a significantly higher tumor burden. This was evident from the larger macroscopic tumor volume (Figure 6B), heavier tumor weight (Figure 6C), and faster tumor growth rate (Figure 6D). These results suggest that CAFs contribute to enhanced tumor growth, potentially affecting patient prognosis.

Enz treatment, significantly inhibited the growth of the 22RV1 xenograft tumors but not the CAF-treated 22RV1 xenograft tumors (Figures 6B–6D), suggesting that CAFs promote resistance to Enz therapy in PCa. Furthermore, the growth of 22RV1 xenografts with or without CAFs was minimally affected by MVC treatment (Figures 6B–6D). However, combined treatment with MVC and Enz significantly reduced the tumor volume of 22RV1 xenografts with CAFs compared to treatment with Enz alone (Figures 6B–6D). Importantly, this combined treatment did not lead to a significant reduction in the body weight of the mice, indicating that it did not increase toxicity *in vivo* (Figure 6E). Moreover, the expression of the proliferation marker Ki67 was reduced and the apoptosis marker cleaved-caspase 3 was significantly increased in 22RV1 xenografts with CAFs when treated with MVC and Enz compared to Enz alone (Figures 6F, S4A, and S4B). Importantly, Immunohistochemistry (IHC) detection showed that CAFs significantly promoted pAKT and AR expression in mouse tumor samples, and MVC significantly blocked the function of CAFs. (Figures 6F, S4C, and S4E).

In conclusion, these results demonstrate the efficacy of the CCR5 antagonist MVC *in vivo* in blocking the promotional effect of CAFs on PCa growth. Furthermore, MVC enhanced the therapeutic effect of Enz in PCa by reversing the Enz-resistant phenotype of PCa cells to an Enz-sensitive phenotype.

CCL5 enhances the expression of PD-L1 in PCa cells

Previous studies have reported a correlation between the formation of a tumor immunosuppressive microenvironment and CAFs.[29] To investigate the potential involvement of CAF-derived CCL5 in immune regulation in PCa, we analyzed the correlation between CCL5 and PD-L1 in the TCGA-PRAD dataset. The results revealed a positive correlation between CCL5 and PD-L1 at the mRNA level (Figure 7A). This suggests that CCL5 plays a role in the expression of PD-L1 in tumors. To further validate these findings, we conducted RT-qPCR, western blot, and flow cytometry were performed. Interestingly, we observed that CCL5 significantly induced a significant increase in both PD-L1 mRNA and protein levels in 22RV1 and C4-2 cells (Figures 7B–7F). Moreover, our analysis of the TCGA-PRAD dataset showed a significant positive correlation between CCR5 and PD-L1 (Figure 7G). This led us to investigate whether CCL5 induces PD-L1 expression via the AKT pathway upon binding to CCR5. Rescue experiments were conducted using the CCR5 antagonist MVC and the AKT inhibitor MK-2206. The findings revealed that both MVC and MK-2206 effectively suppressed the expression of PD-L1 induced by CCL5 (Figures 7H–7J). These results suggest that CCL5 plays a crucial role in the transcription of PD-L1 in PCa and that the inhibition of CCR5 by MVC and AKT by MK-2206 can impede this process. In conclusion, CAFs have the potential to activate the AKT pathway through the CCL5-CCR5 paracrine axis, leading to the upregulation of PD-L1 expression in PCa and subsequent immune evasion.

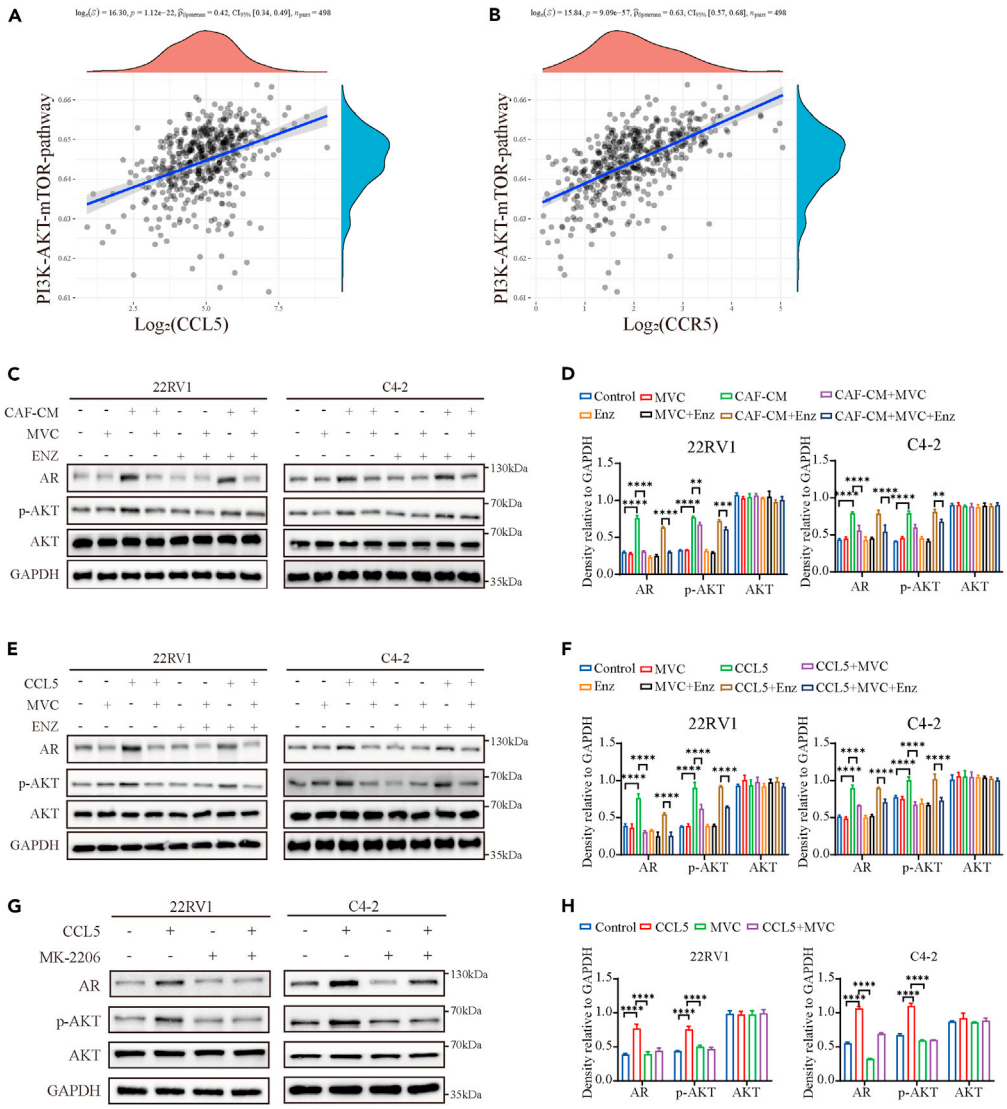

Figure 5. CCL5-CCR5 paracrine signaling activates AKT/AR signaling in PCa cells in order to potentiate Enz resistance

(A and B) Correlation analysis of CCL5 level (A) or CCR5 level (B) and PI3K/AKT/mTOR pathway in TCGA database.

(C and D) Representative western blot image and quantification of phosphorylated AKT (Ser473), AKT, and AR in 22RV1 and C4-2 cells with indicated treatments. 22RV1 and C4-2 cells were pretreated with MVC (1 μM) or DMSO for 1 h, followed by CAF-CM stimulation for 24 h. Western blot analyses were performed 24 h after Enz (10 μM) treatment. $n = 3$ biologically independent CAFs samples.

(E and F) Representative western blot image and quantification of phosphorylated AKT (Ser473), AKT, and AR in 22RV1 and C4-2 cells with indicated treatments. 22RV1 and C4-2 cells were pretreated with MVC (1 μM) or DMSO for 1 h, followed by CCL5 (20 ng/mL) stimulation for 24 h. Western blot analyses were performed 24 h after Enz (10 μM) treatment ($n = 3$).

(G and H) Representative western blot image and quantification of phosphorylated AKT (Ser473), AKT, and AR in 22RV1 and C4-2 cells, which were pretreated with the AKT inhibitor (MK-2206 500 nM) for 1 h, and then treated with CCL5 (20 ng/mL) or PBS for 24 h ($n = 3$). Data are reported as the Mean ± SEM. *$p < 0.05$, **$p < 0.01$, ***$p < 0.001$, ****$p < 0.0001$. One-way ANOVA with Tukey's test for pairwise comparisons for statistical significance analysis in Figures 5D, 5F, and 5H.

DISCUSSION

After an initial positive response to ADT, PCa can progress to lethal drug-resistant PCa or CRPC.[4,6,11] Increasing evidence suggests that the TME plays a crucial role in anti-androgen resistance and immune evasion,[13,14] particularly in the context of resistance to various targeted therapies.[30] This study showed that the presence of CAFs can enhance the expression of AR and contribute to resistance against Enz. CAFs secrete CCL5, which stimulates PCa cells to express high levels of CCR5, forming an important paracrine signal. Blocking the CCL5-CCR5 signaling pathway significantly reduced the tumor-protective effect of CAFs and improved the therapeutic efficacy of Enz. Our study provides new insights into the role of CAFs in the progression of PCa and emphasizes the critical role of

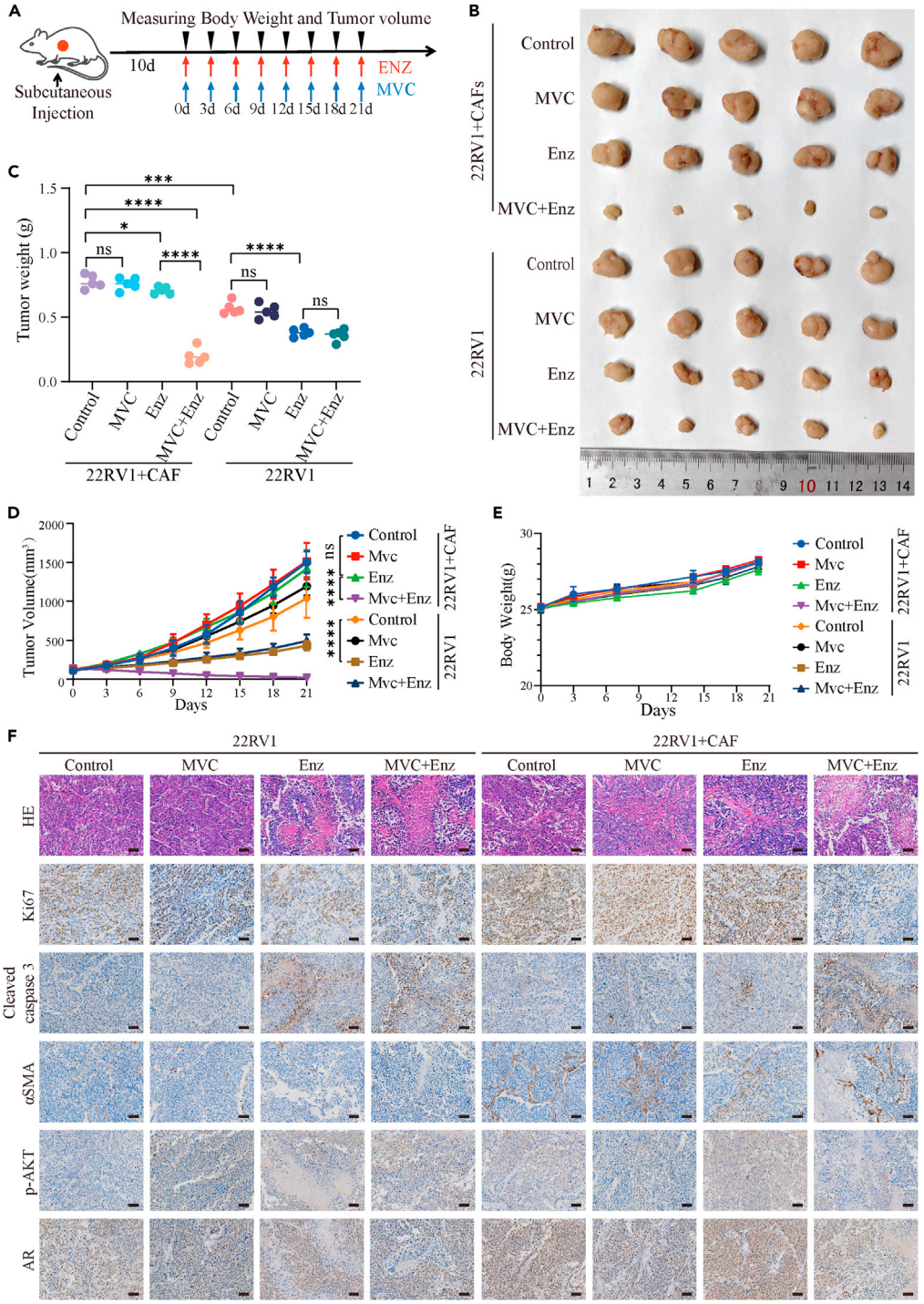

Figure 6. MVC combines with Enz to effectively impair PCa growth

(A) Schematic diagram of the combined treatment of MVC and Enz in nude mice bearing 22RV1 xenografes. MVC (10 mg/kg, i.p.) and Enz (10 mg/kg, i.p.) were given every 3 days from Day 10. The growth of 22RV1 xenografts was monitored, and the tumor volume and body weight were measured every three days.

(B) *In vivo* images of surgically dissected tumors in indicated groups.

(C) The weight of tumors in the indicated groups were measured after the tumors were surgically dissected. The results are showed as the means ± standard deviation (SD) of values (n = 5).

(D) The volume of tumors in indicated groups, measured every 3 days. The results are shown as the means ± SD of values (n = 5).

Figure 6. *Continued*

(E) The body weight in indicated groups, measured every 3 days. The results are showed as the means ± SD of values (n = 5).

(F) Representative images of HE, Ki67, cleaved-caspase 3, α-SMA, *p*-AKT, and AR expression in tumors of the indicated groups, examined by IHC. Scale bar: 20 μm. Data are reported as the Mean ± SEM. ns: no significance, *$p < 0.05$, **$p < 0.01$, ***$p < 0.001$, ****$p < 0.0001$. One-way ANOVA with Tukey's test for pairwise comparisons for statistical significance analysis in Figure 6C. Two-way ANOVA for statistical significance analysis in Figure 6D.

the CCL5-CCR5 paracrine axis in mediating interactions between CAFs and PCa cells, suggesting its potential as a target for sensitizing ADT.

CCL5, derived from CAFs, has been found to promote tumor progression and drug resistance in certain solid tumors.[31,32] Studies have also shown that CCL5 secreted by tumor-associated macrophages (TAMs) in metastatic PCa, can significantly enhance the migration, invasion, and epithelial-mesenchymal transition (EMT) of PCa cells, as well as the self-renewal of prostate cancer stem cells (PCSCs) *in vitro*.[33] These findings suggested that the origin of CCL5 varies at different stages of PCa progression. However, the direct effect of CCL5 on signaling pathways in PCa and its role in the early stages of tumor malignancy remain unclear. We discovered that CCL5 can upregulate AR expression in PCa cells. Resistance to ADT in PCa primarily occurs through activation of the AR signaling axis, which includes amplification of the AR gene and enhancer, AR mutation, and AR splicing variation.[34–36] These mechanisms suggest that persistent activation of AR signaling plays a crucial role in the progression of PCa to CRPC and regulates various malignant characteristics. In terms of functionality, inhibiting the activity of CCR5 using pharmacological methods significantly reduced the resistance of PCa to ADT mediated by CCL5. This rendered the tumor microenvironment/ecosystem highly responsive to CCR5 inhibition.

Recent studies have indicated that T cell interactions with intrinsic AR can hinder the activity of interferon gamma (IFNγ), thus limiting the effectiveness of anti-tumor immunity.[37] However, AR inhibition can sensitize tumors to checkpoint blockade by enhancing $CD8^+$ T cell function. Furthermore, it has been observed that the AR signaling pathway is significantly activated in TAMs of both mouse and human PCa.[38] Suppression of AR leads to the overexpression of TAMs and the secretion of interleukin 1β (IL-1β), which in turn induces the accumulation of myeloid-derived suppressor cells (MDSCs), resulting in an immunosuppressive TME. Therefore, further research is necessary to investigate the impact of CCL5 secreted by CAFs on the expression of AR in different cells within the TME and its potential biological effects.

A recent study showed that CAF-derived nerve growth factor-1 (NRG-1) activates HER3, leading to drug resistance after ADT.[19] Additionally, our previous study revealed that CRPC-associated $SPP1^+$ myCAFs activate ERK signaling in a paracrine manner against ADT.[39] However, our sequencing results showed no difference in NRG1 or SPP1 expression between NFs and CAFs, possibly because our CAFs were derived from drug-naive patients with PCa. Consequently, we concluded that $CCL5^+$ CAFs, $NRG1^+$ CAFs, and $SPP1^+$ CAFs likely represent distinct subpopulations. $CCL5^+$ CAFs may play a role in the induction phase of ADT resistance, whereas $NRG1^+$ CAFs and $SPP1^+$ CAFs may become more significant with prolonged ADT treatment. Therefore, further research on the plasticity and unique functions of CAFs in the TME is necessary to understand their evolving roles during antiandrogen therapy.

ICIs targeting PD-1/PD-L1 have shown great potential in the treatment of specific malignant tumors, but have proven ineffective in PCa treatment.[7–9] Therefore, understanding the regulatory mechanisms underlying PD-L1 expression is crucial. The TME has been widely recognized as a critical factor influencing the efficacy of tumor immunotherapy, with particular attention being paid to CAFs in recent years. Previous studies revealed that CAFs may develop resistance to PD-1/PD-L1 immunotherapy through various mechanisms and pathways.[40] CAFs influence immune cell recruitment and activity by modulating extracellular matrix (ECM) remodeling.[41] They secrete TGF-β, interleukin 6 (IL-6), CXC chemokine ligand 2 (CXCL2), collagen, and other factors, thereby promoting immune cell differentiation and enhancing immune resistance.[42]

The dysregulation of signaling pathways in CAFs is one of the key factors in the occurrence and development of cancer.[43] RNA-seq results show that in addition to the upregulation of the cytokine-cytokine receptor interaction pathway in CAFs, pathways such as NF-κB signaling pathway, IL-17 signaling pathway, TNF signaling pathway, and Hippo signaling pathway are also significantly upregulated in CAFs. Activation of these pathways also plays an important role in tumor progression. The NF-kappa pathway in CAFs of skin cancer, breast cancer, ovarian cancer, and pancreatic cancer regulates cancer progression and promotes treatment resistance by regulating inflammatory factors and a series of chemokines and cytokines in the TME,[43] this may be an important reason for the increased secretion of CCL5 by CAFs. The Hippo signaling pathway in CAFs regulates the metabolic crosstalk between CAFs and cancer cells and regulates the metabolic reprogramming of cancer cells to support cancer progression.[44] Interestingly, IL-17 and TNF-α can also upregulate the expression of PD-L1 in human PCa cells.[45] Therefore, the specific reasons and mechanisms of activation of these important signaling pathways in CAFs need to be further studied.

In addition, CAFs play a role in the accumulation of regulatory T cells.[46] Through experiments conducted on melanoma and CRC, it was observed that CAFs induce the upregulation of tumor PD-L1 via the CXCL5-CXCR2 axis.[47] Our study further supports these findings by demonstrating that CAFs induce the upregulation of PD-L1 in PCa through the AKT pathway, specifically via the CCL5-CCR5 paracrine mechanism, thereby promoting tumor progression. In conclusion, these results highlight the significance of CAFs as an important component of the TME, as they stimulate immune and tumor cells through the secretion of various cytokines and activation of distinct signaling pathways, ultimately affecting the effectiveness of immunotherapy.

In this study, we propose a therapeutic strategy with significant potential for the treatment of advanced PCa. Our approach involves combining Enz therapy with the targeting of the CCL5-CCR5 paracrine mechanism in CAFs. We anticipate that this combined treatment will lead to improved outcomes in patients undergoing ADT. Additionally, our research provides evidence that CAFs may play a role in promoting PD-L1 signaling in PCa. Based on these findings, we propose that the combination of targeted CAFs therapy and ICIs is a promising strategy for treating advanced PCa.

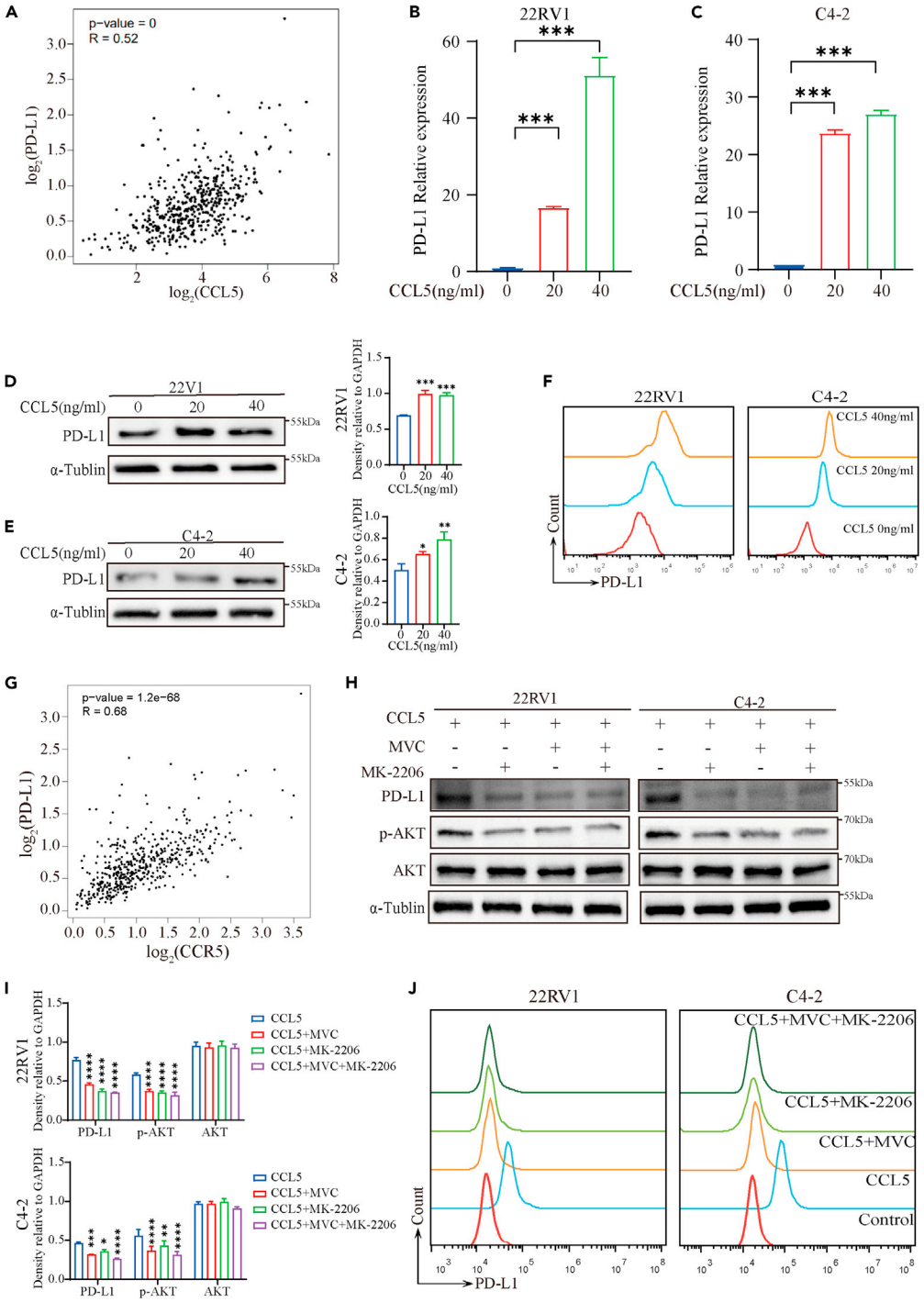

Figure 7. CCL5-CCR5 paracrine signaling activates AKT signaling in PCa cells to induced PD-L1 expression

(A) Pearson correlation analysis of CCL5 level and PD-L1 in the TCGA cohort.

(B and C) The RT-qPCR analysis showing that CCL5 increased the mRNA expression of PD-L1 in 22RV1 and C4-2 cells (n = 3).

(D and E) Representative western blot image and quantification showing that CCL5 increased the protein level of PD-L1 in 22RV1 and C4-2 cells (n = 3).

(F) Flow cytometric analysis showing that CCL5 increased the mRNA expression of PD-L1 in 22RV1 and C4-2 cells (n = 3).

(G) Pearson correlation analysis of CCR5 level and PD-L1 in TCGA cohort.

Figure 7. *Continued*

(H and I) Representative western blot image and quantification of phosphorylated-AKT (Ser473), AKT and PD-L1 in 22RV1 and C4-2 cells pretreated with CCL5 (20 ng/mL) followed by the treatment of the CCR5 inhibitor MVC (1 μM) or AKT inhibitor MK-2206 (500 nM) ($n = 3$).

(J) Flow cytometric analysis showing that phosphorylated-AKT (Ser473), AKT, and PD-L1 in 22RV1 and C4-2 cells pretreated with CCL5 (20 ng/mL) followed by the treatment of the CCR5 inhibitor MVC (1 μM) or AKT inhibitor MK-2206 (500 nM) ($n = 3$). Data are reported as the Mean ± SEM. *$p < 0.05$, **$p < 0.01$, ***$p < 0.001$, ****$p < 0.0001$. One-way ANOVA with Tukey's test for pairwise comparisons for statistical significance analysis in Figures 7B–7D and 7I.

Limitations of the study

Our work reveals that Enz combined with MVC is a combination treatment strategy with great potential for advanced prostate cancer. However, there are not many *in vivo* experimental data in this study, and a larger animal set is needed in further studies.

STAR★METHODS

Detailed methods are provided in the online version of this paper and include the following:

- KEY RESOURCES TABLE
- RESOURCE AVAILABILITY
  - Lead contact
  - Materials availability
  - Data and code availability
- EXPERIMENTAL MODEL AND STUDY PARTICIPANT DETAILS
  - Primary PCa specimens and isolation of primary fibroblasts
  - Cells lines
  - Animal studies
- METHOD DETAILS
  - Conditioned media collection
  - Immunofluorescence analysis
  - Enzyme-linked immunosorbent assay (ELISA)
  - Flow cytometric analysis
  - Cell survival analysis
  - Western blot
  - RNA isolation and qRT-PCR
  - siRNA transient transfection
  - RNA-seq analysis
  - Bioinformatic analyses of human PCa from the TCGA database
  - IHC
- QUANTIFICATION AND STATISTICAL ANALYSIS

SUPPLEMENTAL INFORMATION

Supplemental information can be found online at https://doi.org/10.1016/j.isci.2024.109674.

ACKNOWLEDGMENTS

This work was supported by the Key R&D Plan of Guangdong Province (no: 2023B1111030006); the National key R&D plan of China (no: 2022YFC3602904); the National Natural Science Foundation of China (no: 81974395, no: 82173036); International Science and technology cooperation project plan of Guangdong Province (no: 2021A0505030085); Sun Yat-Sen University Clinical Research 5010 Program (no: 2019005); Beijing Bethune Charitable Foundation (no: mnzl202001); Guangzhou Science and Technology Key R&D Project (no: 202206010117); Beijing Xisike Clinical Oncology Research Foundation (no: Y-MSDZD2022-0760, no: Y-tongshu2021/ms-0162); Supported by the open research funds from the Sixth Affiliated Hospital of Guangzhou Medical University, Qingyuan People's Hospital to Hai Huang. This study was supported by the National Natural Science Foundation of China (no: 82173088), Natural Science Foundation of Guangdong (no: 2022A1515012383), the Guangzhou Science and Technology Fund (no: A202201011299), Baiqiuen Fund, Fundamental Research Funds for the Central Universities, Sun Yat-sen University to Kaiwen Li.

AUTHOR CONTRIBUTIONS

H.H. and Z.X. conceptualized the experiment; Z.X., S.L.Y., and Z.X.X. designed and performed the experiment, analyzed the data, and wrote the manuscript; R.L.Z., S.R.P., and Q.W. performed the experiment; Z.G., B.H.L., and J.J.X. performed the experiment and analyzed the data; K.W.L. supervised the project, provided results interpretation. All the authors read and approved the final manuscript.

DECLARATION OF INTERESTS

The authors declare no competing interests.

Received: October 21, 2023
Revised: January 31, 2024
Accepted: April 3, 2024
Published: April 4, 2024

REFERENCES

1. Siegel, R.L., Miller, K.D., Wagle, N.S., and Jemal, A. (2023). Cancer statistics, 2023. CA A Cancer J. Clin. *73*, 17–48. https://doi.org/10.3322/caac.21763.
2. Katzenwadel, A., and Wolf, P. (2015). Androgen deprivation of prostate cancer: Leading to a therapeutic dead end. Cancer Lett. *367*, 12–17. https://doi.org/10.1016/j.canlet.2015.06.021.
3. Wong, Y.N.S., Ferraldeschi, R., Attard, G., and de Bono, J. (2014). Evolution of androgen receptor targeted therapy for advanced prostate cancer. Nat. Rev. Clin. Oncol. *11*, 365–376. https://doi.org/10.1038/nrclinonc.2014.72.
4. Chi, K., Hotte, S.J., Joshua, A.M., North, S., Wyatt, A.W., Collins, L.L., and Saad, F. (2015). Treatment of mCRPC in the AR-axis-targeted therapy-resistant state. Ann. Oncol. *26*, 2044–2056. https://doi.org/10.1093/annonc/mdv267.
5. Watson, P.A., Arora, V.K., and Sawyers, C.L. (2015). Emerging mechanisms of resistance to androgen receptor inhibitors in prostate cancer. Nat. Rev. Cancer *15*, 701–711. https://doi.org/10.1038/nrc4016.
6. Montgomery, B., Tretiakova, M.S., Joshua, A.M., Gleave, M.E., Fleshner, N., Bubley, G.J., Mostaghel, E.A., Chi, K.N., Lin, D.W., Sanda, M., et al. (2017). Neoadjuvant Enzalutamide Prior to Prostatectomy. Clin. Cancer Res. *23*, 2169–2176. https://doi.org/10.1158/1078-0432.CCR-16-1357.
7. Comiskey, M.C., Dallos, M.C., and Drake, C.G. (2018). Immunotherapy in Prostate Cancer: Teaching an Old Dog New Tricks. Curr. Oncol. Rep. *20*, 75. https://doi.org/10.1007/s11912-018-0712-z.
8. King, A. (2022). Could immunotherapy finally break through in prostate cancer? Nature *609*, S42–S44. https://doi.org/10.1038/d41586-022-02861-y.
9. Venturini, N.J., and Drake, C.G. (2019). Immunotherapy for Prostate Cancer. Cold Spring Harb. Perspect. Med. *9*, a030627. https://doi.org/10.1101/cshperspect.a030627.
10. Antonarakis, E.S., Lu, C., Wang, H., Luber, B., Nakazawa, M., Roeser, J.C., Chen, Y., Mohammad, T.A., Chen, Y., Fedor, H.L., et al. (2014). AR-V7 and resistance to enzalutamide and abiraterone in prostate cancer. N. Engl. J. Med. *371*, 1028–1038. https://doi.org/10.1056/NEJMoa1315815.
11. Claessens, F., Helsen, C., Prekovic, S., Van den Broeck, T., Spans, L., Van Poppel, H., and Joniau, S. (2014). Emerging mechanisms of enzalutamide resistance in prostate cancer. Nat. Rev. Urol. *11*, 712–716. https://doi.org/10.1038/nrurol.2014.243.
12. Shah, N., Wang, P., Wongvipat, J., Karthaus, W.R., Abida, W., Armenia, J., Rockowitz, S., Drier, Y., Bernstein, B.E., Long, H.W., et al. (2017). Regulation of the glucocorticoid receptor via a BET-dependent enhancer drives antiandrogen resistance in prostate cancer. Elife *6*, e27861. https://doi.org/10.7554/eLife.27861.
13. Chen, X., and Song, E. (2022). The theory of tumor ecosystem. Cancer Commun. *42*, 587–608. https://doi.org/10.1002/cac2.12316.
14. Liotta, L.A., and Kohn, E.C. (2001). The microenvironment of the tumour-host interface. Nature *411*, 375–379. https://doi.org/10.1038/35077241.
15. Mueller, M.M., and Fusenig, N.E. (2004). Friends or foes - bipolar effects of the tumour stroma in cancer. Nat. Rev. Cancer *4*, 839–849. https://doi.org/10.1038/nrc1477.
16. Ammirante, M., Luo, J.L., Grivennikov, S., Nedospasov, S., and Karin, M. (2010). B-cell-derived lymphotoxin promotes castration-resistant prostate cancer. Nature *464*, 302–305. https://doi.org/10.1038/nature08782.
17. Calcinotto, A., Spataro, C., Zagato, E., Di Mitri, D., Gil, V., Crespo, M., De Bernardis, G., Losa, M., Mirenda, M., Pasquini, E., et al. (2018). IL-23 secreted by myeloid cells drives castration-resistant prostate cancer. Nature *559*, 363–369. https://doi.org/10.1038/s41586-018-0266-0.
18. Bluemn, E.G., Coleman, I.M., Lucas, J.M., Coleman, R.T., Hernandez-Lopez, S., Tharakan, R., Bianchi-Frias, D., Dumpit, R.F., Kaipainen, A., Corella, A.N., et al. (2017). Androgen Receptor Pathway-Independent Prostate Cancer Is Sustained through FGF Signaling. Cancer Cell *32*, 474–489.e6. https://doi.org/10.1016/j.ccell.2017.09.003.
19. Zhang, Z., Karthaus, W.R., Lee, Y.S., Gao, V.R., Wu, C., Russo, J.W., Liu, M., Mota, J.M., Abida, W., Linton, E., et al. (2020). Tumor Microenvironment-Derived NRG1 Promotes Antiandrogen Resistance in Prostate Cancer. Cancer Cell *38*, 279–296.e9. https://doi.org/10.1016/j.ccell.2020.06.005.
20. Madar, S., Goldstein, I., and Rotter, V. (2013). 'Cancer associated fibroblasts'–more than meets the eye. Trends Mol. Med. *19*, 447–453. https://doi.org/10.1016/j.molmed.2013.05.004.
21. Mishra, D., and Banerjee, D. (2023). Secretome of Stromal Cancer-Associated Fibroblasts (CAFs): Relevance in Cancer. Cells *12*, 628. https://doi.org/10.3390/cells12040628.
22. Kalluri, R., and Zeisberg, M. (2006). Fibroblasts in cancer. Nat. Rev. Cancer *6*, 392–401. https://doi.org/10.1038/nrc1877.
23. Chhabra, Y., and Weeraratna, A.T. (2023). Fibroblasts in cancer: Unity in heterogeneity. Cell *186*, 1580–1609. https://doi.org/10.1016/j.cell.2023.03.016.
24. Kalluri, R. (2016). The biology and function of fibroblasts in cancer. Nat. Rev. Cancer *16*, 582–598. https://doi.org/10.1038/nrc.2016.73.
25. Ishii, G., Ochiai, A., and Neri, S. (2016). Phenotypic and functional heterogeneity of cancer-associated fibroblast within the tumor microenvironment. Adv. Drug Deliv. Rev. *99*, 186–196. https://doi.org/10.1016/j.addr.2015.07.007.
26. Tan, Q., Zhu, Y., Li, J., Chen, Z., Han, G.W., Kufareva, I., Li, T., Ma, L., Fenalti, G., Li, J., et al. (2013). Structure of the CCR5 chemokine receptor-HIV entry inhibitor maraviroc complex. Science *341*, 1387–1390. https://doi.org/10.1126/science.1241475.
27. Tortorella, E., Giantulli, S., Sciarra, A., and Silvestri, I. (2023). AR and PI3K/AKT in Prostate Cancer: A Tale of Two Interconnected Pathways. Int. J. Mol. Sci. *24*, 2046. https://doi.org/10.3390/ijms24032046.
28. Zhang, X.N., Yang, K.D., Chen, C., He, Z.C., Wang, Q.H., Feng, H., Lv, S.Q., Wang, Y., Mao, M., Liu, Q., et al. (2021). Pericytes augment glioblastoma cell resistance to temozolomide through CCL5-CCR5 paracrine signaling. Cell Res. *31*, 1072–1087. https://doi.org/10.1038/s41422-021-00528-3.
29. Arpinati, L., and Scherz-Shouval, R. (2023). From gatekeepers to providers: regulation of immune functions by cancer-associated fibroblasts. Trends Cancer *9*, 421–443. https://doi.org/10.1016/j.trecan.2023.01.007.
30. Sahai, E., Astsaturov, I., Cukierman, E., DeNardo, D.G., Egeblad, M., Evans, R.M., Fearon, D., Greten, F.R., Hingorani, S.R., Hunter, T., et al. (2020). A framework for advancing our understanding of cancer-associated fibroblasts. Nat. Rev. Cancer *20*, 174–186. https://doi.org/10.1038/s41568-019-0238-1.
31. Sun, X., and Chen, Z. (2021). Cancer-associated fibroblast-derived CCL5 contributes to cisplatin resistance in A549 NSCLC cells partially through upregulation of lncRNA HOTAIR expression. Oncol. Lett. *22*, 696. https://doi.org/10.3892/ol.2021.12957.
32. Xu, H., Zhao, J., Li, J., Zhu, Z., Cui, Z., Liu, R., Lu, R., Yao, Z., and Xu, Q. (2022). Cancer associated fibroblast-derived CCL5 promotes hepatocellular carcinoma metastasis through activating HIF1alpha/ZEB1 axis. Cell Death Dis. *13*, 478. https://doi.org/10.1038/s41419-022-04935-1.
33. Huang, R., Wang, S., Wang, N., Zheng, Y., Zhou, J., Yang, B., Wang, X., Zhang, J., Guo, L., Wang, S., et al. (2020). CCL5 derived from tumor-associated macrophages promotes prostate cancer stem cells and metastasis via activating beta-catenin/STAT3 signaling. Cell Death Dis. *11*, 234. https://doi.org/10.1038/s41419-020-2435-y.
34. Dai, C., Heemers, H., and Sharifi, N. (2017). Androgen Signaling in Prostate Cancer. Cold Spring Harb. Perspect. Med. *7*, a030452. https://doi.org/10.1101/cshperspect.a030452.
35. Feng, Q., and He, B. (2019). Androgen Receptor Signaling in the Development of

Castration-Resistant Prostate Cancer. Front. Oncol. *9*, 858. https://doi.org/10.3389/fonc.2019.00858.

36. Viswanathan, S.R., Ha, G., Hoff, A.M., Wala, J.A., Carrot-Zhang, J., Whelan, C.W., Haradhvala, N.J., Freeman, S.S., Reed, S.C., Rhoades, J., et al. (2018). Structural Alterations Driving Castration-Resistant Prostate Cancer Revealed by Linked-Read Genome Sequencing. Cell *174*, 433–447.e19. https://doi.org/10.1016/j.cell.2018.05.036.
37. Guan, X., Polesso, F., Wang, C., Sehrawat, A., Hawkins, R.M., Murray, S.E., Thomas, G.V., Caruso, B., Thompson, R.F., Wood, M.A., et al. (2022). Androgen receptor activity in T cells limits checkpoint blockade efficacy. Nature *606*, 791–796. https://doi.org/10.1038/s41586-022-04522-6.
38. Wang, D., Cheng, C., Chen, X., Wang, J., Liu, K., Jing, N., Xu, P., Xi, X., Sun, Y., Ji, Z., et al. (2023). IL-1beta Is an Androgen-Responsive Target in Macrophages for Immunotherapy of Prostate Cancer. Adv. Sci. *10*, e2206889. https://doi.org/10.1002/advs.202206889.
39. Wang, H., Li, N., Liu, Q., Guo, J., Pan, Q., Cheng, B., Xu, J., Dong, B., Yang, G., Yang, B., et al. (2023). Antiandrogen treatment induces stromal cell reprogramming to promote castration resistance in prostate cancer. Cancer Cell *41*, 1345–1362.e9. https://doi.org/10.1016/j.ccell.2023.05.016.
40. Pei, L., Liu, Y., Liu, L., Gao, S., Gao, X., Feng, Y., Sun, Z., Zhang, Y., and Wang, C. (2023). Roles of cancer-associated fibroblasts (CAFs) in anti- PD-1/PD-L1 immunotherapy for solid cancers. Mol. Cancer *22*, *29*. https://doi.org/10.1186/s12943-023-01731-z.
41. Harper, J., and Sainson, R.C.A. (2014). Regulation of the anti-tumour immune response by cancer-associated fibroblasts. Semin. Cancer Biol. *25*, 69–77. https://doi.org/10.1016/j.semcancer.2013.12.005.
42. Mao, X., Xu, J., Wang, W., Liang, C., Hua, J., Liu, J., Zhang, B., Meng, Q., Yu, X., and Shi, S. (2021). Crosstalk between cancer-associated fibroblasts and immune cells in the tumor microenvironment: new findings and future perspectives. Mol. Cancer *20*, 131. https://doi.org/10.1186/s12943-021-01428-1.
43. Fang, Z., Meng, Q., Xu, J., Wang, W., Zhang, B., Liu, J., Liang, C., Hua, J., Zhao, Y., Yu, X., and Shi, S. (2023). Signaling pathways in cancer-associated fibroblasts: recent advances and future perspectives. Cancer Commun. *43*, 3–41. https://doi.org/10.1002/cac2.12392.
44. Bertero, T., Oldham, W.M., Grasset, E.M., Bourget, I., Boulter, E., Pisano, S., Hofman, P., Bellvert, F., Meneguzzi, G., Bulavin, D.V., et al. (2019). Tumor-Stroma Mechanics Coordinate Amino Acid Availability to Sustain Tumor Growth and Malignancy. Cell Metabol. *29*, 124–140.e10. https://doi.org/10.1016/j.cmet.2018.09.012.
45. Wang, X., Yang, L., Huang, F., Zhang, Q., Liu, S., Ma, L., and You, Z. (2017). Inflammatory cytokines IL-17 and TNF-alpha up-regulate PD-L1 expression in human prostate and colon cancer cells. Immunol. Lett. *184*, 7–14. https://doi.org/10.1016/j.imlet.2017.02.006.
46. McAndrews, K.M., Chen, Y., Darpolor, J.K., Zheng, X., Yang, S., Carstens, J.L., Li, B., Wang, H., Miyake, T., Correa de Sampaio, P., et al. (2022). Identification of Functional Heterogeneity of Carcinoma-Associated Fibroblasts with Distinct IL6-Mediated Therapy Resistance in Pancreatic Cancer. Cancer Discov. *12*, 1580–1597. https://doi.org/10.1158/2159-8290.CD-20-1484.
47. Li, Z., Zhou, J., Zhang, J., Li, S., Wang, H., and Du, J. (2019). Cancer-associated fibroblasts promote PD-L1 expression in mice cancer cells via secreting CXCL5. Int. J. Cancer *145*, 1946–1957. https://doi.org/10.1002/ijc.32278.
48. Sharon, Y., Alon, L., Glanz, S., Servais, C., and Erez, N. (2013). Isolation of normal and cancer-associated fibroblasts from fresh tissues by Fluorescence Activated Cell Sorting (FACS). J. Vis. Exp. *e4425*, e4425. https://doi.org/10.3791/4425.
49. Li, Z., Wang, Q., Peng, S., Yao, K., Chen, J., Tao, Y., Gao, Z., Wang, F., Li, H., Cai, W., et al. (2020). The metastatic promoter DEPDC1B induces epithelial-mesenchymal transition and promotes prostate cancer cell proliferation via Rac1-PAK1 signaling. Clin. Transl. Med. *10*, e191. https://doi.org/10.1002/ctm2.191.

STAR★METHODS

KEY RESOURCES TABLE

REAGENT or RESOURCE	SOURCE	IDENTIFIER
Antibodies		
FITC anti-human CD326 (EpCAM)	Biolegend	Cat#369813; RRID:AB_2650909
APC anti-human CD140a (PDGFRα)	Biolegend	Cat#323511; RRID:AB_2783190
FITC anti-human CD45	4A Biotech	Cat#FHF045-01
PE anti-human CD31	4A Biotech	Cat#FHP031-01
APC Anti-Human PD-L1 (B7-H1)	Proteintech	Cat#APC-65081; RRID:AB_2882979
α-Smooth Muscle Actin (D4K9N) XP® Rabbit mAb	Cell Signaling Technology	Cat#19245; RRID:AB_2734735
Vimentin (D21H3) XP® Rabbit mAb	Cell Signaling Technology	Cat#5741; RRID:AB_10695459
Anti-PDGFR alpha antibody	Abcam	Cat#ab203491; RRID:AB_2892065
Fibroblast activation protein-α (FAP) Rabbit mAb	Abclonal	Cat#A11572; RRID:AB_2861600
Akt (pan) (C67E7) Rabbit mAb	Cell Signaling Technology	Cat#4691; RRID:AB_915783
Phospho-Akt (Ser473) (D9E) XP® Rabbit mAb	Cell Signaling Technology	Cat#4060; RRID:AB_2315049
Androgen Receptor Rabbit mAb	Abclonal	Cat#A19611; RRID:AB_2862699
PD-L1/CD274 Monoclonal antibody	Proteintech	Cat#66248; RRID:AB_2756526
GAPDH Rabbit mAb	Abclonal	Cat#A19056; RRID:AB_2862549
Recombinant Anti- alpha Tubulin antibody	Servicebio	Cat#GB15201
Anti -Ki67 Rabbit pAb	Servicebio	Cat#GB111499; RRID:AB_2927572
Anti -Cleaved- Caspase-3 Rabbit pAb	Servicebio	Cat#GB11532
RANTES Polyclonal antibody	Proteintech	Cat#12000-1-AP; RRID:AB_2877815
Human CCL5/RANTES Antibody	R&D	Cat#AF-278-SP; RRID:AB_354440
HyperFluor™ 488 Goat Anti-Rabbit IgG (H+L) Antibody	APExBIO	Cat#K1206
FITC Goat Anti-Mouse IgG (H+L) Antibody	APExBIO	Cat#K1201
Cy3 Goat Anti-Mouse IgG (H+L) Antibody	APExBIO	Cat#K1207
HRP Goat Anti-Rabbit IgG (H+L) Antibody	APExBIO	Cat#K1223
Chemicals, peptides, and recombinant proteins		
Recombinant Human RANTES (CCL5)	PeproTech	Cat#AF-300-06
MK-2206 AKT inhibitor	Selleck Chemicals	Cat#S1078
Maraviroc	Selleck Chemicals	Cat#S2003
Enzalutamide	Selleck Chemicals	Cat#S1250
Collagenase, Type 1	Worthington	Cat#LS004194
RPMI 1640 media	Gibco	Cat#C11875
DMEM media	Gibco	Cat#C11995
Penicillin-Streptomycin (10,000 U/mL)	Gibco	Cat#15140
Phosphate-Buffered Saline	procell	Cat#PB180327
Fetal Bovine Serum	ExCell Bio	Cat#FSP500
DMSO	Solarbio	Cat#D8371
Matrigel Matrix	Corning	Cat#354262
DAPI	Beyotime	Cat#C1006
Tris (Hydroxymethyl) Aminomethane	Biosharp	Cat#BS083
Glycine	Biosharp	Cat#BS082
SKim Milk	Biofroxx	Cat#1172

(*Continued on next page*)

Continued

REAGENT or RESOURCE	SOURCE	IDENTIFIER
Sodium dodecyl sulfate	Biofroxx	Cat#3250
Bovine Serum Albumin	servicebio	Cat#GC305010
5XSDS-PAGE running buffer	Beyotime	Cat#P0286
One-Step PAGE Gel Fast Preparation Kit	EpiZyme	Cat#PG212
180 kDa Prestained Protein Marker	ThermoFisher	Cat#26617
Invitrogen™ Lipofectamine™ RNAiMAX	Invitrogen	Cat#13778150
Cell Counting Kit-8 (CCK-8)	APExBIO	Cat#K1018
Protease Inhibitor Cocktail (100x)	Cwbiotech	Cat#CW2200S
Phosphatase Inhibitor Cockail (100x)	Cwbiotech	Cat#CW2383S
RNA Quick Purification kit	ESscience	Cat#RN001
Trizol	ThermoFisher	Cat#15596
PEG300	Selleck Chemicals	Cat#S6704
Tween80	Selleck Chemicals	Cat#S6702
RIPA Lysis Buffer	Beyotime	Cat#P0013B
BCA Protein Assay Kit	Beyotime	Cat#P0011
Critical commercial assays		
C-C Motif Chemokine Ligand 5 ELISA Kit	J&L Biological	Cat#JL11689
Annexin V-FITC/PI Apoptosis Kit	Elabscience	Cat#E-CK-A211
ChamQ Universal SYBR qPCR Master Mix	Vazyme	Cat#Q711
HiScript III All-in-one RT SuperMix Perfect for qPCR	Vazyme	Cat#R333
Deposited data		
Raw and analyzed data	This paper	NODE: OEP005133
Experimental models: Cell lines		
Human: 22RV1	ATCC	Cat#CRL-2505
Human: C4-2	ATCC	Cat#CRL-3314
Human: PC3	ATCC	Cat#CRL-1435
Human: DU145	ATCC	Cat#HTB81
Human: LNCAP	ATCC	Cat#CRL-17
Human: VCAP	ATCC	Cat#CRL-2876
Experimental models: Organisms/strains		
BALB/c-Nude	Gempharmatech	N/A
Oligonucleotides		
Primers for CCL5, CCR5, PD-L1, GAPDH, see Table S1	This paper	N/A
siRNA targeting sequence: CCL5, CCR5. see Table S2	This paper	N/A
Software and algorithms		
Image Studio software	LICOR	N/A
GraphPad Prism version 8.0 for Windows	GraphPad Software	N/A
Illumina NovaSeq 6000 platform	Novogene	N/A
Flowjo software v10	BD	N/A
Beckman CtoFLEX S Software	Beckman	N/A
Excel	Microsoft	N/A
Other		
PVDF paper	Merck millipore	Cat#ISEQ00010

RESOURCE AVAILABILITY

Lead contact

Further information and requests for resources and reagents should be directed to and will be fulfilled by the lead contact, Dr. Hai Huang (huangh9@mail.sysu.edu.cn).

Materials availability

This study did not generate new unique reagents.

Data and code availability

- RNA-sequencing data that support the findings of this study have been deposited into the National Omics Data Encyclopedia (NODE) with the accession code OEP005133 (https://www.biosino.org/node/project/detail/OEP005133). The transcriptomic data for PCa samples used for correlation analysis is publicly available from TCGA database (https://tcga-data.nci.nih.gov/tcga). All data presented in this study will be shared upon reasonable request by the lead contact, Dr. Hai Huang (huangh9@mail.sysu.edu.cn).
- This paper does not report any original code.
- Additional information required to reanalyze the data reported in this paper is available from the lead contact upon request.

EXPERIMENTAL MODEL AND STUDY PARTICIPANT DETAILS

Primary PCa specimens and isolation of primary fibroblasts

The Ethics Committees of the Sun Yat-sen University's Sun Yat-sen Memorial Hospital approved the use of human specimens in this study (approval no. SYSEC-KY-KS-2020-201). Human PCa tissues and their corresponding normal prostate tissues (at least 5 cm away from the tumor) were obtained from the Sun Yat-sen Memorial Hospital Sun Yat-sen University (Guangzhou, China). The patients or their guardians provided informed consent, and prior therapy was not administered to any individual. Two pathologists made histopathological diagnoses of the PCa specimens. The tissue samples involved in this study are all derived from Asian Han male patients with PCa.

Fibroblasts were isolated as previously described.[48] To summarize, the tumours and non-tumour tissues underwent mincing and dissociation in RPMI-1640 supplemented with 0.5% collagenase Type I for a duration of 2 h at 37°C. Subsequently, they were cultured in a humidified atmosphere at 37°C with 5% CO2 using RPMI-1640 supplemented with 10% FBS until the fibroblasts adhered to the culture dish. Fibroblasts were used at less than 18 passages.

Cells lines

The human PCa cell line, 22RV1, C4-2, LNCAP, VCAP, PC3, and DU145 were purchased from the CAS Center for Excellence in Molecular Cell Science (Shanghai, China). CAFs and NFs were isolated from PCa tumor tissues and adjacent non-tumor tissues, respectively. Cells were cultured in RPMI-1640 medium containing 10% fetal bovine serum (FBS) and 1% penicillin-streptomycin. In addition, polymerase chain reaction (PCR) was performed to confirm the absence of mycoplasma contamination.

Animal studies

The use of animals in this study was approved by the Institutional Animal Care and Use Committee of the Sun Yat-sen University (approval no. SYSU-IACUC-2021-000041). A total of 2×10^6 22RV1 cells were either combined or not combined with the same quantity of CAFs at a 1:1 ratio in a 100 μl solution of PBS mixed with Matrigel at a 1:1 proportion. This mixture was administered subcutaneously to 4-week-old male BALB/c nude mice. After 10 days, when the tumor size reached approximately 100 mm^3 (defined as day 0), the mice were randomly divided into eight groups (n = 5) and received the following treatment. To determine the effect of CAFs on ENZ treatment, mice were treated three days with control (10% DMSO + 40% PEG300 +5% Tween80 + 45% ddH2O, i.p.), ENZ (10 mg/kg, i.p.), MVC (10 mg/kg, i.p.) or a combination of ENZ and MVC. Tumour sizes ($V = \text{length} \times \text{width}^2 \times 0.5$) and body weight were evaluated by monitoring every three days. On the 22nd day after xenograft treatment, the animals were euthanized and the tumors were collected for further investigation.

METHOD DETAILS

Conditioned media collection

On the first day of the experiment, NFs, CAFs, or PCa cells were plated in a 10 cm dish. The following day, the cells were washed twice in PBS, followed by addition of serum-free media. On the third day, the first conditioned medium was collected and replaced with serum-free medium. On the fourth day, the conditioned medium was collected for a second time. We combined the collections for the treatment to the tumor cells. To eliminate any cell debris, we employed a 0.45 μm filter and stored the filtered conditioned media either at 4°C for 7 days or -80°C for 3 months.

Immunofluorescence analysis

NFs and CAFs were seeded a cover glass at approximately 60% confluence. After a 24 h incubation period, the cellular samples were fixed using 4% PFA for 20 min, followed by three consecutive 5 min washes with PBS. To ensure effective permeabilization, the cells were treated

with 0.1% Triton X-100 and subsequently blocked in a solution of 3% BSA in PBS for 1 hour at 37°C. Next, the slides were incubated in primary antibodies diluted in PBS containing 1% FBS overnight at 4°C. Next morning, the cells were washed in PBS for 5 minutes three times to remove excess antibodies. To detect the presence of the target proteins, secondary antibodies were diluted in PBS (1:200) and applied to the samples for 20 minutes at 37°C. DAPI (20 mg/ml) was used to label the cell nuclei. Fluorescence images were obtained using a ZEISS LSM710 laser scanning confocal microscope and ZEN 2.3 software.

Enzyme-linked immunosorbent assay (ELISA)

The concentrations of CCL5 in CAFs, NFs, 22RV1, C4-2, LNCAP, VCAP, PC3, and DU145 conditioned media were evaluated using human CCL5 uncoated ELISA kits, according to the manufacturer's instructions.

Flow cytometric analysis

Briefly, NFs, CAFs, 22RV1, or C4-2 were labeled with FITC-conjugated anti-EPCAM antibody, FITC-conjugated anti-CD45 antibody, PE-conjugated anti-CD31 antibody, PE-conjugated anti-PDGFRα antibody, or APC-conjugated anti-PD-L1 antibody at room temperature for 30 min.

Various compounds were used to treat 22RV1 or C4-2 cells, with DMSO serving as the vehicle control for the drugs at a final concentration not exceeding 0.1%. Following treatment, the cells were collected and stained with a solution containing 1x Annexin V binding buffer, fluorochrome-conjugated annexin V, and DAPI at room temperature for 15 min, followed by flow cytometric analysis using a Beckman CtoFLEX S. Data were analyzed using Beckman CtoFLEX S software and FlowJo software v10 (FlowJo).

Cell survival analysis

PCa cell survival was assessed using the Cell Counting Kit (CCK-8). Briefly, cells were seeded in a 96-well plate at a density of 1.5×10^3 cells/well and treated as described in the figures. CCK8 was added to each well every 2 h. The absorbance was measured at 450 nm.

Western blot

Cell lysates were obtained using RIPA Lysis Buffer supplemented with 1% protease inhibitor cocktail and 1% phosphatase inhibitor cocktail. To determine the protein concentration, a BCA Protein Assay Kit was used following the manufacturer's instructions. The proteins were combined with 5x SDS-PAGE Protein Sample Loading Buffer and heated at 95°C for 10 min. The boiled protein samples were then preserved at -80°C until required for further experimentation. The proteins were separated on pre-cast gels, along with a Full-range Rainbow protein marker. The gels were run using a self-made 1x running buffer at 120 V. Proteins were transferred to PVDF paper that had been activated in 100% methanol. The transfer was conducted in a self-made 1x transfer buffer at 4°C for 2 h at 250 mA. Subsequently, the membrane was blocked with 5% nonfat milk for a period of 1 h before the addition of the primary antibody. Afterward, the membrane was washed with a self-prepared 1X TBST solution. Antibodies used for immunoblot assays were as follows: Anti-αSMA, Anti-Vimentin, Anti-PDGFRα, Anti-FAP, Anti-AKT, Anti-pAKT-Ser473, Anti-AR, anti-PD-L1, anti-GAPDH, anti-αTubulin. The next day, membranes were incubated with HRP-conjugated secondary antibodies and immunoreactions were visualized and imaged by a SmartChemiTM system (SAGE, China). Band intensities were quantified via ImageJ software.

RNA isolation and qRT-PCR

Extraction and isolation of total RNA was performed using an RNA-Quick purification kit, according to the manufacturer's instructions. Subsequently, RNA was diluted to a concentration of below 500 ng/μL in DEPC-treated water. A qPCR SYBR Green Master Mix and cDNA SuperMix kit were used for RT-PCR. The mRNA expression levels of the genes were detected using the ABI Quanstudio DX Real-Time PCR System. Table S2 provides a detailed list of all the primers employed in this study.

siRNA transient transfection

To silence, RNA interference was performed using specific siRNA oligonucleotides targeting CCL5 and CCR5 (or no-target control siRNAs) from GenePharma (Suzhou, China). The cells were transiently transfected with siRNA using Lipofectamine RNAiMAX, and the culture medium was replaced after 24 h. The effectiveness of gene silencing was evaluated using RT-PCR at 48 h post-transfection. The Table S3 lists the target sequences of the siRNAs used in the experiments.

RNA-seq analysis

Total RNA was extracted using TRIzol reagent. Novogene (Beijing, China) was used to construct the cDNA library. An Illumina NovaSeq 6000 platform (Illumina, Novogene) was used for RNA-seq. RNA-seq data were analyzed using the R package (DESeq).

Bioinformatic analyses of human PCa from the TCGA database

The TCGA database (https://tcga-data.nci.nih.gov/tcga) was used for bioinformatic analyses of human PCa. Gene expression differences were determined using GEPIA (http://gepia2.cancer-pku.cn). Gene correlation analysis was performed using Home-for-Researchers Analysis software (https://www.home-for-researchers.com).

IHC

Tumor and normal tissues were fixed in 10% formalin, paraffin-embedded using a standard protocol, then cut into 5 μm sections, which were stored at room temperature. H&E staining and immunohistochemistry were performed as previously described.[49] Images were acquired and processed using a Nikon Ni-U microscope and the NIS-Elements software.

QUANTIFICATION AND STATISTICAL ANALYSIS

Data were obtained from three independent experiments, in experiments that required the use of CAFs supernatants, 3 of the 16 CAFs were randomly used for biological independent experiments. For comparisons between two groups, two-tailed unpaired T test was applied. For comparisons among three or more groups, one-way analysis of variance (ANOVA) followed by Tukey's multiple comparisons and two-way ANOVA followed by Tukey's multiple comparisons was applied. GraphPad Prism (version 8.0) was used for statistical analyses. Quantified values were presented as the mean ± SD. Statistical significance was set at $P < 0.05$ (ns: no significance, *$P < 0.05$, **$P < 0.01$, and ***$P < 0.001$, ****$P < 0.0001$).